

# Myeloid EGFR deficiency accelerates recovery from AKI via macrophage efferocytosis and neutrophil apoptosis

Received: 1 March 2024

Accepted: 19 April 2025

Published online: 16 May 2025



Yu Pan<sup>1,2,3,6</sup>, Shirong Cao<sup>1,2,6</sup>, Yinqiu Wang<sup>1,2,6</sup>, Jiaqi Tang<sup>1,2</sup>, Aolei Niu<sup>1,2</sup>, Sarah Abu Kar<sup>1,2</sup>, Mengdi Jiang<sup>1,2</sup>, Fenfen Peng<sup>1,2</sup>, Gabriela M. Siew<sup>1,2</sup>, Wentian Lu<sup>1,2</sup>, Suwan Wang<sup>1,2</sup>, Matthew Wilson <sup>1,2,4</sup>, Craig Brooks<sup>1,2</sup>, Agnes B. Fogo<sup>5</sup>, Andrew S. Terker <sup>1,2</sup>, Juan Pablo Arroyo Ornelas <sup>1,2</sup>, Jianchun Chen<sup>1,2</sup>, Ming-Zhi Zhang<sup>1,2</sup>  & Raymond C. Harris <sup>1,2,4</sup> 


Altered expression and activation of Epidermal Growth Factor Receptor (EGFR) is implicated in acute and chronic kidney injury. One of the important cellular sources of EGFR is the myeloid compartment, which plays roles in both acute kidney injury and subsequent fibrosis. Here we show in a murine ischemic acute kidney injury (AKI) model that myeloid deletion of EGFR promotes a pro-resolving, anti-inflammatory phenotype and increased efferocytotic capacity in macrophages. This leads to accelerated recovery in response to AKI and inhibited subsequent development of tubulointerstitial fibrosis. We find that selective EGFR deletion in neutrophils also accelerates recovery from ischemic kidney injury and reduces subsequent fibrosis. EGFR activation plays an essential role in increasing the life span of neutrophils in the injured kidney. Deletion of EGFR expression either in all murine myeloid cells or selectively in neutrophils decreases kidney neutrophil Mcl-1 expression and promotes neutrophil apoptosis, which is accompanied by accelerated recovery from organ injury and reduced subsequent fibrosis. These studies thus identify coordinated and complementary roles for EGFR activation in neutrophils and macrophages to exacerbate kidney injury.

The epidermal growth factor receptor (EGFR) is activated by a family of ligands that includes EGF, TGF- $\alpha$ , HB-EGF, amphiregulin, betacellulin, epigen and epiregulin<sup>1</sup>, as well as activation by non-receptor signaling pathways<sup>2</sup>. EGFR activation induces phosphorylation of its intrinsic kinase domain and subsequent phosphorylation of specific tyrosine residues within the cytoplasmic tail, which serve as docking sites for a variety of signaling molecules. Receptor activation mediates well-described cellular responses, including dedifferentiation, proliferation,

and cell viability<sup>3,4</sup>. Alterations in EGFR expression and activation have been implicated in responses to acute and chronic injury in a variety of organs, including the kidney. We and others have previously reported that proximal tubule EGFR expression is an important mediator of recovery from acute ischemic kidney injury, but aberrant persistent EGFR activation can induce progressive tubulointerstitial fibrosis<sup>5–11</sup>.

Myeloid-derived cells play important roles in the propagation of acute kidney injury and in either subsequent recovery from injury or

<sup>1</sup>Division of Nephrology and Hypertension, Department of Medicine, Vanderbilt University Medical Center, Nashville, TN, USA. <sup>2</sup>Vanderbilt Center for Kidney Disease, Vanderbilt University Medical Center, Nashville, TN, USA. <sup>3</sup>Division of Nephrology, Shanghai Ninth People's Hospital, Shanghai Jiao Tong University School of Medicine, Shanghai, China. <sup>4</sup>Department of Veterans Affairs Hospital, Nashville, TN, USA. <sup>5</sup>Department of Pathology, Microbiology and Immunology, Vanderbilt University Medical Center, Nashville, TN, USA. <sup>6</sup>These authors contributed equally: Yu Pan, Shirong Cao, Yinqiu Wang.

 e-mail: [ming-zhi.zhang@vumc.org](mailto:ming-zhi.zhang@vumc.org); [ray.harris@vumc.org](mailto:ray.harris@vumc.org)

development of progressive organ damage<sup>12–16</sup>. EGFR activation mediates chemotaxis in monocytes and proliferation in macrophages in vitro<sup>17</sup>. Selective deletion of EGFR in cells of myeloid origin in experimental models of colitis led to reduced colonic inflammation<sup>18,19</sup>. However, to date the role of EGFR activation in different myeloid cell subtypes has not been investigated in response to acute kidney injury.

Although proinflammatory monocytes/macrophages mediate further continued inflammation and tissue injury following kidney injury due to ischemia or toxins, neutrophils are the initial myeloid-derived cell type responding to acute kidney injury. Neutrophils exacerbate the initial epithelial and endothelial cell injury in the kidney but subsequently facilitate recovery by undergoing apoptosis and promoting the conversion of proinflammatory macrophages to an anti-inflammatory, proresolving phenotype as a result of the efferocytosis of the apoptotic neutrophils<sup>20</sup>. Although it has been previously reported that neutrophils also express EGFR<sup>21</sup>, the role of EGFR in neutrophil responses in acute kidney injury has not been previously investigated. We now report that EGFR deletion in all myeloid cells as well as selective deletion in neutrophils leads to accelerated recovery from acute kidney injury and reduced development of subsequent tubulointerstitial fibrosis.

## Results

### Mouse with selective myeloid EGFR deletion had accelerated recovery after ischemic injury and less subsequent post-ischemic renal fibrosis

To determine the potential role of myeloid EGFR in acute kidney injury (AKI), we employed CD11b-Cre: EGFR<sup>fl/fl</sup> (myeloid EGFR<sup>-/-</sup>) mice and EGFR<sup>fl/fl</sup> (WT) mice<sup>11,22</sup> and subjected these mice to ischemia/reperfusion kidney injury (Fig. 1A). The effectiveness of myeloid EGFR deletion in myeloid EGFR<sup>-/-</sup> mice was confirmed by qPCR analysis showing decreased EGFR mRNA expression in isolated macrophages and neutrophils as well as immunofluorescent staining showing decreased EGFR protein expression in both macrophages (CD68 and EGFR colocalization) and neutrophils (S100A9 and EGFR colocalization) after ischemic injury (Supplementary Fig. S1A). Although the initial injury was comparable between myeloid EGFR<sup>-/-</sup> and WT mice, selective myeloid EGFR deletion led to accelerated functional recovery from the ischemic insult (Fig. 1B). Three days after ischemic injury, myeloid EGFR<sup>-/-</sup> mice exhibited less tubular injury (Fig. 1C). Four weeks after ischemic injury, myeloid EGFR<sup>-/-</sup> mouse kidneys had less infiltration of macrophages (Fig. 1D, E) and lymphocytes (Supplementary Fig. S1B), lower levels of proinflammatory cytokines/chemokines in kidney tissue (Fig. 1F) and in isolated macrophages (Supplementary Fig. S1C) and less renal fibrosis, as indicated by lower mRNA and protein expression of profibrotic and fibrotic components, including  $\alpha$ -SMA, collagen I, collagen IV, TGF- $\beta$ , fibronectin, CTGF, PDGFR- $\beta$  and vimentin and less quantitative Picrosirius-red staining (Fig. 1G–I and Supplementary Fig. S1D).

### Selective myeloid EGFR deletion did not affect monocyte infiltration into ischemic kidneys

As the number of kidney macrophages was markedly lower in myeloid EGFR<sup>-/-</sup> mice than WT mice four weeks after ischemic injury, we investigated whether EGFR deletion affected the ability of blood monocytes to infiltrate the kidney in response to ischemic injury. We used flow cytometry analysis to analyze alterations of blood monocytes and kidney monocytes at early time points after initial injury. There were comparable progressive decreases in blood monocytes in WT mice and myeloid EGFR<sup>-/-</sup> mice at 4 and 16 h after ischemic injury and similar progressive increases in kidney monocytes (Supplementary Fig. 2A). We also isolated bone marrow derived monocytes (BMDMs) from WT and myeloid EGFR<sup>-/-</sup> mice, labeled WT BMDMs with the monocyte tracking dye PKH26 and EGFR<sup>-/-</sup> BMDMs with the monocyte tracking dye PKH67 and injected a mixture containing equal

amounts of labeled WT and EGFR<sup>-/-</sup> BMDMs ( $1 \times 10^6$  for each labeled cell type) retro-orbitally into WT recipients immediately after ischemic kidney injury<sup>23</sup>. The pedicle of the left recipient mouse kidney was clamped for 35 min to ensure sufficient ischemic injury. To confirm that the infiltration of labeled BMDMs into the injured kidney was the result of the injury and not due to random homing, the contralateral (right) kidney was left intact as a control to compare BMDM infiltration into the uninjured kidney compared to the injured kidney and to avoid mortality because of the severe ischemic injury. Mice were sacrificed 24 h and 48 h after the ischemic insult. The number of infiltrated PKH26 WT BMDMs and PKH67 EGFR<sup>-/-</sup> BMDMs was similar in both contralateral kidneys and injured kidneys at 24 and 48 h, although the infiltrated BMDMs were >10-fold higher in injured kidneys than in contralateral intact kidneys (Supplementary Fig. S2B–D). The total labeled BMDMs did not significantly increase from 24 to 48 h in contralateral intact kidneys but did significantly increase in injured kidneys (percentage of kidney cells:  $0.0292 \pm 0.0180$  vs.  $0.0152 \pm 0.0019$ ,  $P < 0.001$ ). These results indicated that selective myeloid EGFR deletion did not affect the ability of BMDMs to home to ischemic kidneys.

### Deletion of EGFR polarized monocytic cells to an anti-inflammatory and pro-resolving phenotype in vivo and in vitro

We compared kidney expression levels of inflammatory cytokines/chemokines between WT and myeloid EGFR<sup>-/-</sup> mice at early time points after ischemic injury. Proinflammatory *Tnf* and *Il6* transcripts were markedly lower in kidneys of myeloid EGFR<sup>-/-</sup> mice than WT mice early after ischemic injury (Supplementary Fig. S3A). In isolated renal macrophages, expression of proinflammatory *Tnf*, *Il1b*, and *Ccl3* mRNA levels were comparable at baseline and 2 h after ischemic injury in myeloid EGFR<sup>-/-</sup> and WT mice, but they were all significantly lower in the myeloid EGFR<sup>-/-</sup> mouse kidney macrophages isolated at 16 h and 72 h after ischemic injury compared to corresponding WT mouse kidney macrophages (Supplementary Fig. S3B). In contrast, macrophage anti-inflammatory and pro-resolving transcripts (*Cd206*, mannose receptor, *Arg1*, and *Ym-1*) were higher in myeloid EGFR<sup>-/-</sup> mice than WT mice 3 days after ischemic injury (Supplementary Fig. S3C), a time point at which macrophages have been reported to have a predominantly pro-reparative phenotype<sup>13,24</sup>. Protein levels of KIM-1 and NGAL, two markers of kidney epithelial injury, were also lower in myeloid EGFR<sup>-/-</sup> mice than WT mice on day 1 after ischemic injury, further validating a protective effect of myeloid EGFR deletion (Supplementary Fig. S3D).

To determine further the role of EGFR in macrophage polarization, we isolated BMDMs from WT and myeloid EGFR<sup>-/-</sup> mice and polarized them to a reparative and anti-inflammatory (“M2”) phenotype with IL-4/IL-13 or a proinflammatory (“M1”) phenotype with LPS/IFN- $\gamma$ <sup>13</sup>. EGFR<sup>-/-</sup> BMDMs had attenuated LPS/IFN- $\gamma$ -induced mRNA expression of proinflammatory M1 cytokines, MCP-1 (CCL2), iNOS and IL-23 (Supplementary Fig. S3E). Although the mRNA levels of TNF- $\alpha$  and IRF5, a transcription factor mediating an M1 phenotype, were numerically higher in EGFR<sup>-/-</sup> BMDMs at baseline compared to WT BMDMs, both TNF- $\alpha$  and IRF5 mRNA levels markedly increased in WT BMDMs with LPS/IFN- $\gamma$ -induced M1 polarization but did not significantly increase in myeloid EGFR<sup>-/-</sup> BMDMs (Supplementary Fig. S3F). In contrast, there was significantly increased expression of IL-4/IL-13-induced markers of M2 polarization in EGFR<sup>-/-</sup> BMDMs compared to WT BMDMs (Supplementary Fig. S3G). We also treated WT BMDMs and EGFR<sup>-/-</sup> BMDMs with an EGFR inhibitor (AG1478) or EGFR agonist (EGF) to evaluate their effect on M1 and M2 polarization. AG1478 decreased LPS/IFN- $\gamma$ -induced proinflammatory cytokine expression while EGF had no effect, suggesting EGFR was already efficiently activated under M1 polarization (Supplementary Fig. S3H). In WT BMDMs, IL-4/IL-13-induced M2 polarization was augmented by AG1478 but inhibited by EGF (Supplementary Fig. S3I). Neither AG1478 nor EGF had any effect on M1 or M2 polarization in EGFR<sup>-/-</sup> BMDMs (Supplementary Fig. S3H, I).

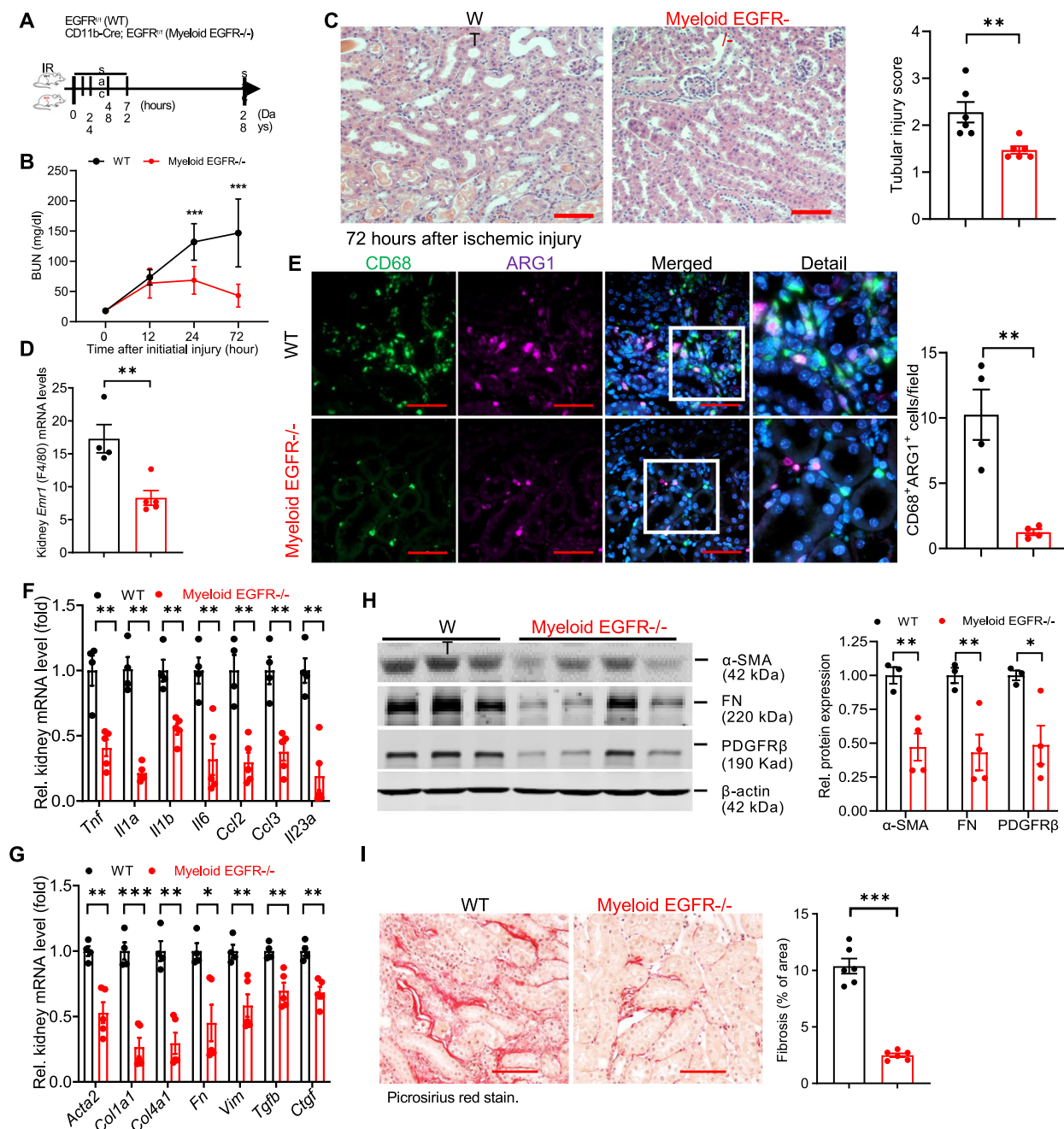


**Fig. 1 | Selective deletion of EGFR in myeloid cells led to accelerated functional recovery after ischemic kidney injury and less post-ischemia renal fibrosis.**

**A** Schematic of experimental protocol with IRI-UNX, indicating unilateral pedicle clamping for 28.5 min plus uninephrectomy. **B** Myeloid EGFR<sup>-/-</sup> had accelerated functional recovery from the ischemic insult, indicated by more rapid BUN decline ( $n = 6, 7$  and  $8$ ). **C** Myeloid EGFR<sup>-/-</sup> mouse kidneys had less tubular injury 3 days after injury ( $n = 6$ ). (**D** and **E**) Myeloid EGFR<sup>-/-</sup> mice had decreased macrophage density, indicated by: **D** lower mRNA levels of F4/80 ( $n = 4$  and  $5$ ) and **E** quantitative

colocalization of CD68 and arginase 1 (ARG1) ( $n = 4$ ). **F** Myeloid EGFR<sup>-/-</sup> mice had lower kidney proinflammatory cytokines/chemokines, including *Tnf*, *Il1a*, *Il1b*, *Il6*, *Ccl2*, *Ccl3* and *Il23a* ( $n = 4$  and  $5$ ). **G–I** Myeloid EGFR<sup>-/-</sup> mice had less kidney fibrosis, indicated by: **G** lower mRNA ( $n = 4$  and  $5$ ) and **H** protein levels ( $n = 3$  and  $4$ ) of profibrotic and fibrotic genes and **I** less Picrosirius red staining ( $n = 6$ ) 4 weeks after initial ischemic injury. Scale bar = 50  $\mu$ m for all. Data are means  $\pm$  SD (**B**) or means  $\pm$  SEM (**C–G**),  $^*P < 0.05$ ,  $^{**}P < 0.01$ ,  $^{***}P < 0.001$ , analyzed using 2-way ANOVA followed by Tukey's post hoc test for (**B**); 2 tailed Student's *t* test (**C–I**).

To gain further insight into the effects of selective EGFR deletion in kidney myeloid cells in response to ischemic injury, we isolated CD45<sup>+</sup> immune cells one and three days after ischemic injury and performed scRNA-seq (Fig. 2A). The isolation process allowed effective segregation of single cell clusters identified as myeloid and lymphocytic subtypes (Fig. 2B). In WT CD45<sup>+</sup> cells, EGFR mRNA expression was predominantly expressed in macrophages and neutrophils (Fig. 2C).

There were 11 subclusters identified that corresponded to macrophages (Fig. 2D)<sup>25–27</sup>. A violin plot of representative genes in each

subcluster indicated resident macrophages (C1qc<sup>High</sup> HP<sup>Low</sup> clusters: 1, 2, 4, 6, 8, 9, 10), infiltrating macrophages (C1qc<sup>Low</sup> HP<sup>High</sup> clusters: 3, 5, 7, 11), proinflammatory macrophages (clusters 7 and 11) and fibrosis-promoting macrophages (clusters 5, 7, 11) (Fig. 2E). Gene Ontology analysis suggested that cluster 6 was associated with macrophage proliferation, clusters 1 and 2 were associated with cell differentiation and small GTPase mediated signal transduction, cluster 10 with energy metabolism and cluster 9 with regulation of the apoptotic signaling pathway (Fig. 2F). Volcano and violin plots indicated myeloid EGFR



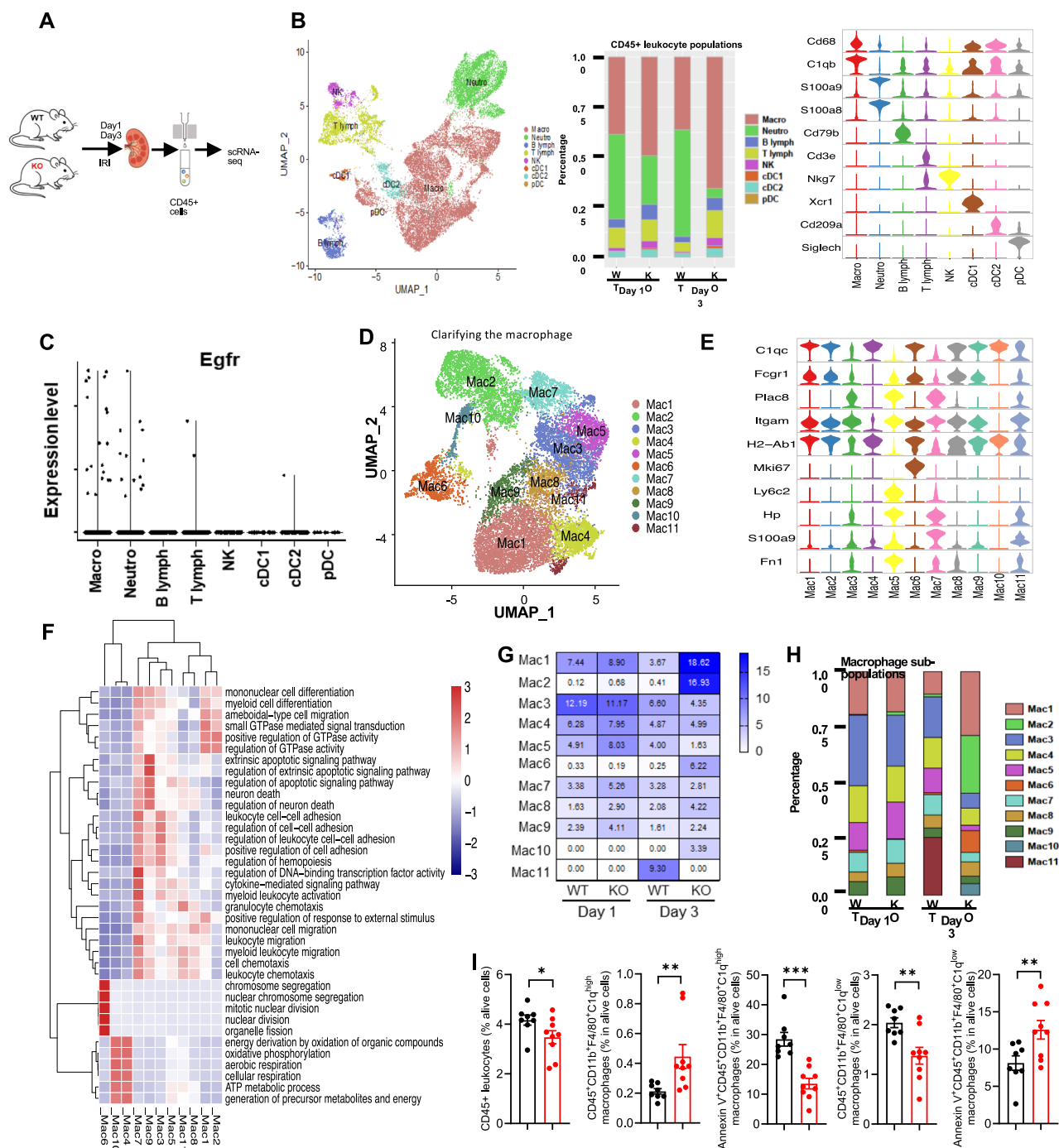


**Fig. 2 | Myeloid EGFR deficiency led to increased resident macrophage sub-clusters but relative decreases in infiltrating macrophages.** **A** Both male *EGFR<sup>fl/fl</sup>* (WT) and *CD11b-Cre:EGFR<sup>fl/fl</sup>* (myeloid *EGFR<sup>-/-</sup>*) mice underwent ischemic injury. The animals were sacrificed at days 1 and 3, and kidney leukocytes were enriched with CD45 microbeads for single cell RNA-seq (scRNA-seq). **B** scRNA-seq analysis identified clusters of kidney cells, and canonical markers of kidney cell populations were used to identify major cell types in the kidney: macrophages (*Cd68*, *C1qb*), neutrophils (*S100a9*, *S100a8*), B lymph cells (*Cd79b*), T lymph cells (*Cd3e*), NK cells (*Nkg7*), cDC1 (*Cd68*, *C1qb*, *Xcr1*), cDC2 (*Cd68*, *C1qb*, *Cd209a*), and pDC (*Siglech*). **C** *Egfr* mRNA was mainly detected in myeloid neutrophils and macrophages in WT mice. **D** Eleven subclusters were identified corresponding to macrophages: Mac1-11. **E** Violin plot of representative genes in each subcluster. *C1qc<sup>high</sup>HP<sup>low</sup>* Mac: Mac1, 2, 4, 6, 8, 9, and 10, which tended to be resident macrophages; *C1qc<sup>low</sup>HP<sup>high</sup>* Mac:

Mac3, 5, 7, and 11, which tended to be infiltration macrophages; proliferating macrophages (Mac 6), proinflammatory macrophages (Mac7 and Mac11) and profibrotic macrophages (Mac 5, 7, and 11). **F** Gene Ontology (GO) analysis suggested that Mac1 and 2 clusters were associated with myeloid cell differentiation and small GTPase mediated signal transduction, Mac10 cluster with energy metabolism and Mac 9 cluster with regulation of apoptotic signaling pathways. **G, H** The percentage of cells in each cluster. Compared to WT mice, myeloid *EGFR<sup>-/-</sup>* mice had significantly increased Mac1, 2, 6, 8, 9 and 10 but not Mac 3, 5, 7, and 11 subclusters. **I** Flow cytometry confirmed that 3 days after ischemic injury myeloid *EGFR<sup>-/-</sup>* mouse kidneys had increased *C1qc<sup>high</sup>HP<sup>low</sup>* resident macrophages with less apoptosis, while the *C1qc<sup>low</sup>HP<sup>high</sup>* infiltrating macrophages were decreased and had increased apoptosis compared to WT mice ( $n = 9$  and  $10$ ). Data are means  $\pm$  SEM,  $^*P < 0.05$ ,  $^{**}P < 0.01$ ,  $^{***}P < 0.001$ , analyzed using 2 tailed Student's *t* test.



deficiency reduced expression of genes in macrophages associated with a proinflammatory phenotype (*Il1b*, *S100a9*), fibrosis (*Vim* and *Fnl1*), and chemotaxis (*Cxcl2*, *Cxcl3*) and increased genes associated with an anti-inflammatory, reparative phenotype (*Adgre1*/F4/80+ and *Mrc1*/Cd206+) (Supplementary Fig. S4A).

Pseudotime trajectory analysis delineated changes in RNA profiles in macrophages from day 1 to day 3 after injury in wild type mice indicating resident macrophage proliferation, differentiation and activation (Mac6-Mac2-Mac1) and recruitment of pro-inflammatory and pro-fibrotic infiltrated macrophages (Mac5-Mac7-Mac3-Mac11), while in myeloid EGFR<sup>-/-</sup> mice, there were predominantly RNA profiles indicating proliferation, differentiation and increases in phagocytic capacity (Mac1, Mac2, Mac6) (Supplementary Fig. S4B, C).

Between days 1 and 3, myeloid EGFR deficiency resulted in increased resident macrophage subclusters (Mac1, Mac2, Mac10) but relative decreases in infiltrating macrophage clusters, in both proinflammatory (Mac11) and fibrosis-promoting clusters (Mac5 and Mac11) (Fig. 2G, H). Flow cytometry also indicated that three days after ischemic injury, myeloid EGFR<sup>-/-</sup> mouse kidney C1q<sup>high</sup>Hp<sup>low</sup> resident macrophages were increased and had less apoptosis (annexin V+) than WT, while the C1q<sup>low</sup>Hp<sup>high</sup> infiltrating macrophages were decreased and had increased apoptosis (Fig. 2I). Therefore, these results indicated that myeloid EGFR deficiency promoted the proliferation, differentiation and survival of the resident macrophage population and increased the energy-intensive activation state of phagocytosis/efferocytosis.

### There were markedly decreased kidney neutrophils following ischemic injury in myeloid EGFR<sup>-/-</sup> mice

scRNA-seq results indicated that the percentage of neutrophils in CD45<sup>+</sup> cells was decreased by more than 40% one day after ischemic injury and was further decreased by more than 90% on day 3 in the myeloid EGFR<sup>-/-</sup> kidneys compared to WT kidneys (Supplementary Fig. S5A). Macrophages made up a greater percentage of CD45<sup>+</sup> myeloid cells in myeloid EGFR<sup>-/-</sup> mice, especially at day 3. Flow cytometry confirmed that kidney CD45<sup>+</sup> leukocytes continued to increase from 2 h to 72 h in WT mice, while myeloid EGFR<sup>-/-</sup> kidney CD45<sup>+</sup> leukocytes increased to similar levels as WT mice 2 h after ischemic injury but then progressively declined (Fig. 3A). Kidney CD45<sup>+</sup>CD11b<sup>+</sup>F4/80<sup>+</sup> macrophages increased to similar levels in WT and myeloid EGFR<sup>-/-</sup> mice after ischemic injury (Fig. 3B). Blood CD45<sup>+</sup>CD11b<sup>+</sup>Gr-1<sup>+</sup> neutrophil levels were similarly increased in WT and myeloid EGFR<sup>-/-</sup> mice after ischemic injury (Supplementary Fig. S5B). Although kidney neutrophils were also similar in WT and myeloid EGFR<sup>-/-</sup> mice 2 h after ischemic injury, there was a continued increase in neutrophil number in WT kidneys but a progressive decline in myeloid EGFR<sup>-/-</sup> kidneys (Fig. 3C). Quantitative immunohistochemical staining with Ly6G/Gr-1 for neutrophils confirmed fewer neutrophils in kidneys of myeloid EGFR<sup>-/-</sup> mice at day 3 after ischemic injury (Supplementary Fig. S5C).

scRNA-seq analysis indicated that there were nine subclusters corresponding to neutrophils (Fig. 3D)<sup>25–27</sup>. Compared to WT mice, myeloid EGFR<sup>-/-</sup> clusters had marked decreases in the percentage of neutrophils in cluster 1, which was associated with activation and migration and in cluster 3, which was associated with activation of TNF- $\alpha$ , IL-17 and NF $\kappa$ B signaling pathways. In contrast EGFR deletion increased the percentage of neutrophils in cluster 2, which was associated with small GTPase-mediated signal transduction and immune cell-cell interactions (Fig. 3E, F).

EGFR immunostaining was low in neutrophils from WT mice at 2 h after ischemic injury but peaked at 16 h and was still elevated at 72 h. As expected, both total numbers of neutrophils and neutrophils with EGFR expression were minimal in myeloid EGFR<sup>-/-</sup> mice, confirming effective deletion of EGFR in neutrophils (Supplementary Fig. S6A–E). Kidneys of myeloid EGFR<sup>-/-</sup> mice one day after injury also had significantly decreased numbers of neutrophils with EGFR activation

(p-EGFR) and a decreased percentage of p-EGFR-positive neutrophils (Supplementary Fig. S6F). In addition, although there was detectable EGFR mRNA in neutrophils isolated with Ly6G microbeads from uninjured WT kidneys, there was essentially undetectable EGFR mRNA in macrophages isolated with F4/80 microbeads. Following ischemic injury, EGFR mRNA levels increased in both macrophages and neutrophils with similar patterns, but the absolute expression level was higher in neutrophils than in macrophages (Supplementary Fig. S6G).

### Mice with selective neutrophil EGFR deletion had accelerated recovery from ischemic injury and less post-ischemic renal fibrosis

To determine the role of neutrophil EGFR in response to kidney injury, we generated mice with selective EGFR deletion in neutrophils (S100A8-Cre: EGFR<sup>fl/fl</sup>, NeutEGFR<sup>-/-</sup>) and corresponding EGFR<sup>fl/fl</sup> (WT) mice. Both qPCR analysis and immunofluorescent staining indicated efficient and selective EGFR deletion in neutrophils but not in macrophages in NeutEGFR<sup>-/-</sup> mouse kidneys after ischemic injury (Supplementary Fig. S7A, B). In addition, baseline kidney inflammatory profiles were comparable between WT and NeutEGFR<sup>-/-</sup> mice (Supplementary Fig. S7C).

After acute ischemia/reperfusion injury, NeutEGFR<sup>-/-</sup> mice had accelerated functional recovery similar to what was observed in myeloid EGFR<sup>-/-</sup> mice (Fig. 4A, B) and had decreased tubular injury and decreased mRNA and protein expression of the injury markers, KIM-1 and NGAL, 16 h after ischemic injury (Fig. 4C and Supplementary Fig. S8A, B). NeutEGFR<sup>-/-</sup> mouse kidneys had decreased CD45<sup>+</sup> leukocytes and CD45<sup>+</sup>CD11b<sup>+</sup>Gr-1<sup>+</sup> neutrophils, while CD45<sup>+</sup>CD11b<sup>+</sup>F4/80<sup>+</sup> kidney macrophages were numerically but not significantly different compared to WT mice (Fig. 4D). One day after ischemic injury, NeutEGFR<sup>-/-</sup> mouse kidney macrophages had increased mRNA expression of pro-resolving and anti-inflammatory cytokines but decreased expression of proinflammatory cytokines (Supplementary Fig. S9A, B), indicating that there were decreased proinflammatory macrophages in NeutEGFR<sup>-/-</sup> kidneys. Quantitative Gr-1 immunostaining confirmed that NeutEGFR<sup>-/-</sup> mice had markedly fewer kidney neutrophils 3 days after ischemic injury compared to WT mice (Supplementary Fig. S9C). A time course of p-EGFR immunostaining in wild type kidneys indicated progressive p-EGFR colocalization in neutrophils from 2 to 16 h following ischemic injury (Fig. 4E, F), while as expected there was minimal p-EGFR in NeutEGFR<sup>-/-</sup> neutrophils (Fig. 4E, G).

To investigate whether selective EGFR deletion in neutrophils had a similar effect as EGFR deletion in all myeloid cells to attenuate development of kidney fibrosis after ischemia injury, NeutEGFR<sup>-/-</sup> mice and corresponding WT mice were subjected to an AKI to CKD model that we have previously described (Fig. 5A)<sup>28</sup>. NeutEGFR<sup>-/-</sup> mice had less kidney injury, as indicated by a decreased tubular injury score (Supplementary Fig. S8C) and lower mRNA levels of KIM-1 (Fig. 5B), in association with less fibrosis, as indicated by lower protein levels of  $\alpha$ -SMA, FN, and PDGFR $\beta$  (Fig. 5C) and lower mRNA levels of profibrotic and fibrotic genes, including *Acta2*, *Tgfb1*, *Col1a1*, *Col3a1*, *Col4a1*, *Fnl1*, *Vim*, and *Ctgf* (Fig. 5D). NeutEGFR<sup>-/-</sup> mouse kidney also had less immune cell infiltration, as indicated by lower mRNA levels of *Emr1*, *Cd68*, *Ly6g* (Fig. 5E), *Cd3*, *Cd4*, and *Cd8* (Supplementary Fig. S10A) and less macrophage and neutrophil infiltration, evaluated by both flow cytometric analysis (Fig. 5F) and quantitative immunostaining (Fig. 5G), in association with lower levels of proinflammatory cytokines (Supplementary Fig. S10B). Quantitative Picrosirius red staining also confirmed less kidney fibrosis in NeutEGFR<sup>-/-</sup> mouse kidneys (Fig. 5G).

### Myeloid EGFR<sup>-/-</sup> mice had increased kidney macrophage efferocytosis after ischemic injury

Gene Ontology analysis indicated that on day 3 after ischemic injury, kidney macrophages from myeloid EGFR<sup>-/-</sup> mice had increased

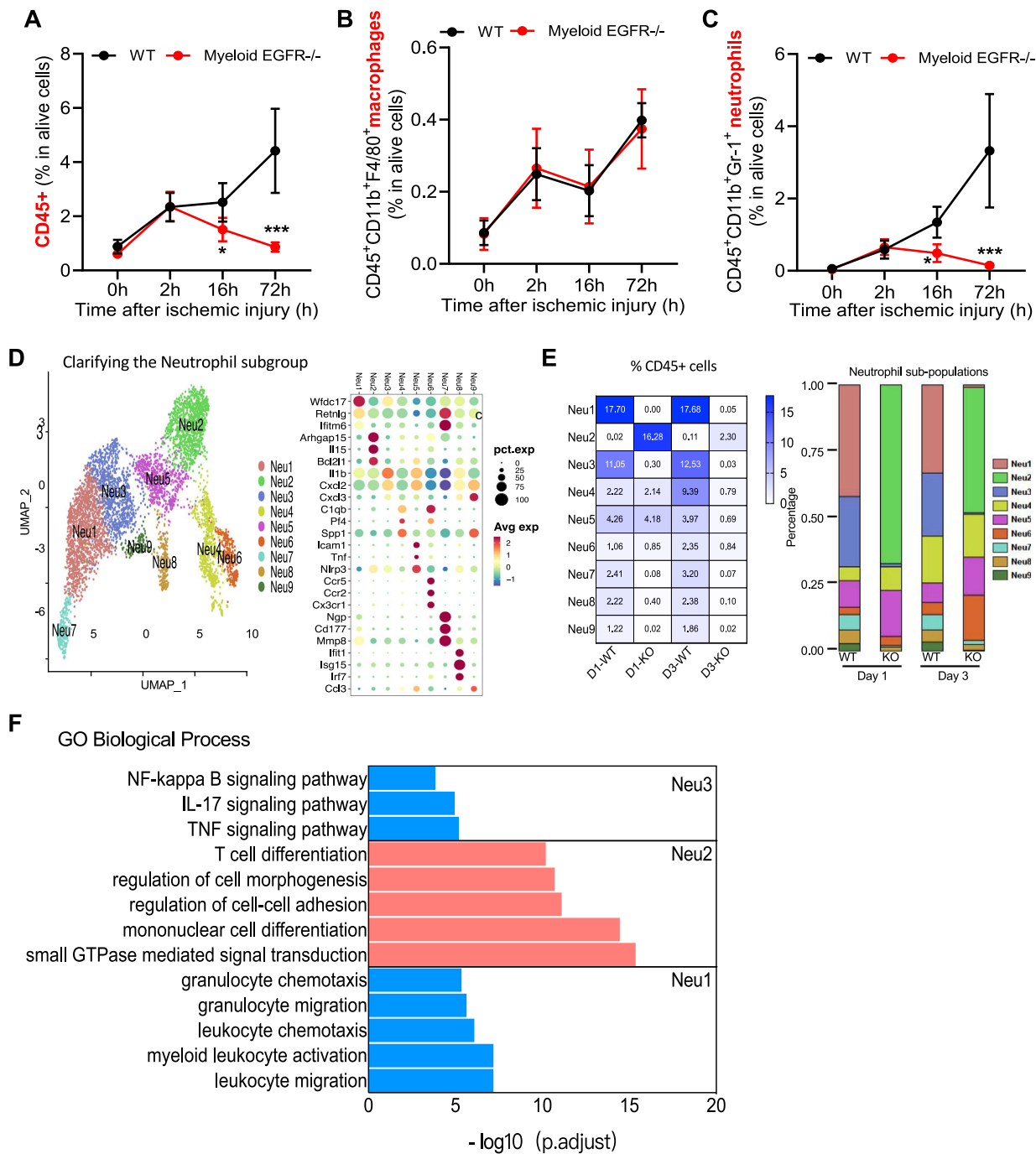
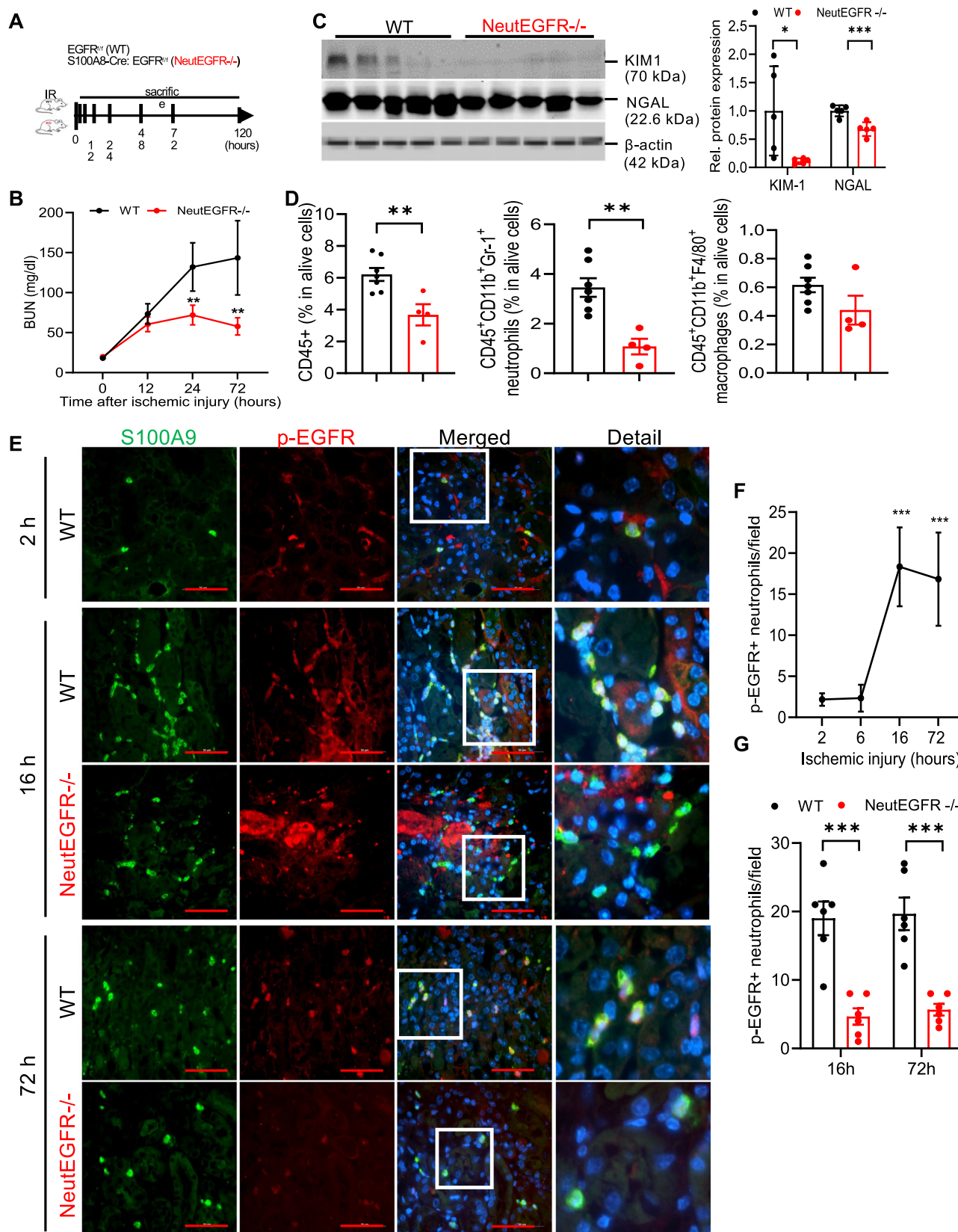


**Fig. 3 | Myeloid EGFR deletion had less kidney neutrophil infiltration after ischemic injury.** Both male EGFR<sup>fl/fl</sup> (WT) and CD11b-Cre: EGFR<sup>fl/fl</sup> (myeloid EGFR<sup>-/-</sup>) mice underwent ischemic injury. Kidney myeloid cells were evaluated with flow cytometry at different time points. **A** Renal CD45<sup>+</sup> leukocytes, **B** CD45<sup>+</sup>CD11b<sup>+</sup>F4/80<sup>+</sup> macrophages and **C** CD45<sup>+</sup>CD11b<sup>+</sup>Gr-1<sup>+</sup> neutrophils were comparable between WT mice and myeloid EGFR<sup>-/-</sup> mice at baseline and 2 h after ischemic injury, but both CD45<sup>+</sup> leukocytes and neutrophils were lower in myeloid EGFR<sup>-/-</sup> mice than WT mice at 16 and 72 h after ischemic injury while macrophages increased to similar amounts ( $n = 5, 6$  and  $7$ ). **D** Nine clusters were identified corresponding to

neutrophils: Neu1-9. Bubble plots showed representative genes for each subcluster. **E** The percentage of cells in each cluster. Compared to WT mice, myeloid EGFR deletion reduced Neu1 and Neu3 clusters but increased Neu2 cluster. **F** Gene Ontology (GO) Biological Process analysis indicated that Neu1 cluster was associated with neutrophil migration, chemotaxis and activation, Neu2 cluster with small GTPase mediated signal transduction and immune cell-cell reaction, and Neu3 cluster with TNF, IL17 and NF- $\kappa$ B signaling pathway activation. Data are means  $\pm$  SD, \* $P < 0.05$ , \*\*\* $P < 0.001$ , analyzed using 2-way ANOVA followed by Tukey's post hoc test for (A–C).

efferocytosis ability, as indicated by increased activity of the GTPase activator guanyl-nucleotide exchange factor and genes associated with endocytosis (Supplementary Fig. S11A). Three days after ischemic injury, myeloid EGFR<sup>-/-</sup> mouse kidney macrophages had increased mRNA levels of proteins involved in efferocytosis, including bridging molecules Gas6, Pros1, and Mfge8 (Supplementary Fig. S11B).

We employed an ex vivo real-time efferocytosis assay to evaluate the effect of EGFR on macrophage efferocytosis ability. Bone marrow derived neutrophils isolated from WT mice were labeled with pHrodo Red, then treated with staurosporine to induce apoptosis. Kidney macrophages were isolated from WT and myeloid EGFR<sup>-/-</sup> mice 2 days after ischemic injury (35 min bilateral pedicle clamping) and seeded in



a 24-well plate in phenol red free 10% DMEM medium for 30 min before pHrodo Red labeled apoptotic neutrophils were added at a 4:1 ratio of apoptotic neutrophils vs. macrophages. Macrophages from myeloid EGFR<sup>-/-</sup> mice after ischemic injury had significantly higher efferocytosis ability compared to WT mice (Fig. 6A).

We also evaluated macrophage efferocytosis with flow cytometry. WT bone marrow neutrophils were stained with CFSE and apoptosis was again induced by staurosporine. Kidney macrophages were isolated as above and stained with CytoTell blue. A mixture of CFSE labeled apoptotic neutrophils and CytoTell blue labeled kidney



**Fig. 4 | Mice with selective EGFR deletion in neutrophils had accelerated functional recovery associated with fewer renal neutrophils after ischemic injury.** **A** Schematic of the experimental protocol with IRI-UNX induced by unilateral pedicle clamping for 28.5 min plus uninephrectomy. **B–D** NeutEGFR<sup>-/-</sup> mice had accelerated functional recovery from the ischemic insult, indicated by more rapid BUN decline ( $n = 4–8$ ) (**B**), lower KIM1 and NGAL protein levels ( $n = 5$ ) (**C**) at day 1 after ischemic injury. **D** Three days after ischemic injury, NeutEGFR<sup>-/-</sup> mice had fewer renal CD45<sup>+</sup> leukocytes and CD45<sup>+</sup>CD11b<sup>+</sup>Gr-1<sup>+</sup> while CD45<sup>+</sup>CD11b<sup>+</sup>F4/80<sup>+</sup>

macrophage numbers were numerically but not significantly different than WT mice ( $n = 4$  and 7). **E–G**: Immunofluorescent staining indicated: **E**, **F** increased numbers of p-EGFR expressing neutrophils ( $n = 6$ ) in WT mice after ischemic injury and (**E**, **G**) significantly fewer p-EGFR<sup>+</sup> neutrophils in NeutEGFR<sup>-/-</sup> mice at 16 and 72 h after ischemic injury ( $n = 6$ ). Scale bar = 50  $\mu$ m. Data are means  $\pm$  SD (**B**, **F**), means  $\pm$  SEM (**C**, **D**, **G**), \* $P < 0.05$ , \*\* $P < 0.01$ , \*\*\* $P < 0.001$ , analyzed using 2-way ANOVA followed by Tukey's post hoc test for **B** and **F**; 2 tailed Student's  $t$  test for (**C**, **D** and **G**).

macrophages (4:1) were plated onto 6-well plates and cultured for 16 h at 37 °C. Efferocytosis was identified in macrophages positive for both CytoTell blue and CFSE with flow cytometry analysis (Fig. 6B). Similar to what was seen in the real-time efferocytosis assay, macrophages from myeloid EGFR<sup>-/-</sup> mice had significantly higher efferocytosis ability compared to WT mice after ischemic injury (Fig. 6C). Unlike the myeloid EGFR<sup>-/-</sup> mice, macrophages isolated from the mice with selective deletion of EGFR in neutrophils had no differences in efferocytosis ability compared to WT mice.

### Selective EGFR deletion in neutrophils increased neutrophil apoptosis

Pseudotime trajectory analysis indicated changes in the mRNA profile in neutrophils from day 1 to day 3 after ischemic injury (Supplementary Fig. S12A). In combination with canonical markers, cluster 1 (*Wfdc17*, *Retnlg*), cluster 3 (*Il1b*, *Cxcl2*, *Cxcl3*) and cluster 7 (*Ngp*, *Cd177*) were associated with neutrophil recruitment, chemotaxis, and activation. Clusters 5 and 9 were involved in promoting inflammation, and cluster 2 was associated with neutrophil apoptosis and activation of other immune cells. On days 1 and 3, deletion of neutrophil EGFR expression in neutrophils inhibited recruitment, activation and proinflammatory responses and enhanced apoptosis and subsequent activation of populations of other immune cells (Supplementary Fig. S12B).

Gene Set Enrichment Analysis (GSEA) indicated that neutrophils with EGFR deficiency had increases in differentially expressed genes associated with the promotion of early cell apoptosis after ischemic injury (Supplementary Fig. S12C). To determine whether kidney neutrophils from either myeloid EGFR<sup>-/-</sup> mice or NeutEGFR<sup>-/-</sup> mice had increased intrinsic propensity to undergo apoptosis, we measured kidney Annexin V positive neutrophils six hours after ischemic injury and found increased annexin V<sup>+</sup> neutrophils in myeloid EGFR<sup>-/-</sup> mice or NeutEGFR<sup>-/-</sup> mice compared to their corresponding WT mice (Supplementary Fig. S13A–C). We also used cleaved caspase-3 flow cytometry to evaluate kidney neutrophil apoptosis at 4 h and 16 h after ischemic injury (Fig. 7A). Four hours after ischemic injury, increased kidney cleaved caspase 3<sup>+</sup> neutrophils were already evident in both myeloid EGFR<sup>-/-</sup> and NeutEGFR<sup>-/-</sup> mouse kidneys compared to corresponding WT mouse kidneys, and increased neutrophil apoptosis was prevented with emricasan, a pan-caspase inhibitor (Supplementary Fig. S14A, B). Sixteen hours after ischemic injury, kidney cleaved caspase 3-positive neutrophils were significantly higher in both myeloid EGFR<sup>-/-</sup> and NeutEGFR<sup>-/-</sup> mouse kidneys compared to corresponding WT mouse kidneys (Fig. 7B). Emricasan treatment caused significant decreases in cleaved caspase-3-positive neutrophils in both myeloid EGFR<sup>-/-</sup> and NeutEGFR<sup>-/-</sup> mouse kidneys, leading to increased kidney neutrophils (Fig. 7B). We also stained neutrophils with cleaved caspase-3 and cleaved caspase-9 in NeutEGFR<sup>-/-</sup> mice with vehicle or emricasan 16 h after ischemic injury. Emricasan-treated NeutEGFR<sup>-/-</sup> mice had more kidney neutrophils compared to vehicle-treated NeutEGFR<sup>-/-</sup> mice, in association with fewer cleaved caspase-3-positive or cleaved caspase-9-positive neutrophils (Fig. 7C and Supplementary Fig. S15A, B). These results indicate that deletion of EGFR in neutrophils predisposed to increased neutrophil apoptosis after ischemic injury.

To investigate the potential role of neutrophil apoptosis in kidney function and development of kidney fibrosis, NeutEGFR<sup>-/-</sup> mice were

treated with vehicle or emricasan for the first 3 days immediately after ischemic injury. Emricasan led to more severe kidney injury as indicated by higher BUN one day after injury as well as more kidney fibrosis 4 weeks later as indicated by increased kidney  $\alpha$ -SMA and quantitative Picrosirius red staining (Supplementary Fig. S16).

We also investigated kidney neutrophil apoptosis after ischemic injury in mice pretreated with the EGFR tyrosine kinase inhibitor, erlotinib. Kidney CD45<sup>+</sup>CD11b<sup>+</sup>Gr-1<sup>+</sup> neutrophils increased to similar levels in vehicle-treated and erlotinib-treated mice at 6 h after ischemic injury. They continued to increase at 24 h in vehicle-treated mice but not in erlotinib-treated mice, while kidney CD45<sup>+</sup>CD11b<sup>+</sup>F4/80<sup>+</sup> macrophages were similar between vehicle and erlotinib-treated mice at 6 h and 24 h after ischemic injury (Supplementary Fig. S17A). Kidney cleaved caspase 3 positive neutrophils were higher in erlotinib-treated mice than in vehicle-treated mice 4 h after bilateral ischemic injury (Supplementary Fig. S17B). These studies indicated that significant neutrophil apoptosis occurred early after ischemic injury with either genetic or pharmacologic inhibition of EGFR pathway.

### EGFR signaling promoted renal neutrophil survival via maintaining antiapoptotic protein Mcl-1 levels after ischemic injury

Mcl-1 belongs to the Bcl-2 family, and neutrophils express anti-apoptotic Mcl-1, but not Bcl-2<sup>29</sup>. When the pro-apoptotic protein, Bax is separated from its binding protein Mcl-1, it initiates the intrinsic apoptotic pathway, with release of cytochrome C and Smac from mitochondria, followed by the activation of caspase cascades and cell apoptosis<sup>30</sup>.

We isolated kidney neutrophils from WT and NeutEGFR<sup>-/-</sup> mice at day 3 after ischemic injury and evaluated mRNA levels of components of the Bcl-2 family. Mcl-1 mRNA was highly expressed in WT neutrophils but was downregulated in NeutEGFR<sup>-/-</sup> neutrophils, while mRNAs of the proapoptotic family members were not significantly different (Supplementary Fig. S18A). A time course indicated that kidney neutrophil Mcl-1 mRNA levels increased gradually after AKI in WT mice, while in NeutEGFR<sup>-/-</sup> mice, the mRNA levels of neutrophil Mcl-1 were markedly lower compared to corresponding neutrophils in WT mice (Supplementary Fig. S18B).

Immunofluorescent staining indicated that on day 3 after AKI, p-EGFR and Mcl-1 colocalized in neutrophils from WT kidney, but expression of both was minimal in neutrophils in NeutEGFR<sup>-/-</sup> mice (Fig. 8A). Immunofluorescent Mcl-1 expression in kidney neutrophils was determined in WT and NeutEGFR<sup>-/-</sup> mice at 0, 2, 6, 16, and 72 h after ischemic injury (Fig. 8B–D and Supplementary Fig. S17). Kidney Mcl-1 expressing neutrophils were comparable between WT and NeutEGFR<sup>-/-</sup> mice at 2 and 6 h after ischemic injury but significantly increased at 16 and 72 h after ischemic injury in WT mice but not in NeutEGFR<sup>-/-</sup> mice (Fig. 8B–D and Supplementary Fig. S19A, B). Administration of EGF in vitro increased immunoreactive Mcl-1 expression in bone marrow neutrophils from WT but not myeloid EGFR<sup>-/-</sup> mice (Fig. 8E). In addition, EGF administration decreased WT bone marrow neutrophil expression of *Noxa*, a pro-apoptotic gene (Supplementary Fig. S19C)<sup>31</sup>. These results indicate that EGFR activation directly upregulated Mcl-1 transcription and expression as well as other apoptotic genes in neutrophils in response to ischemic injury.

We pretreated WT mice with an Mcl-1 inhibitor, SC3845, and subjected these mice to ischemic injury for 16 h. Mcl-1 inhibition led to

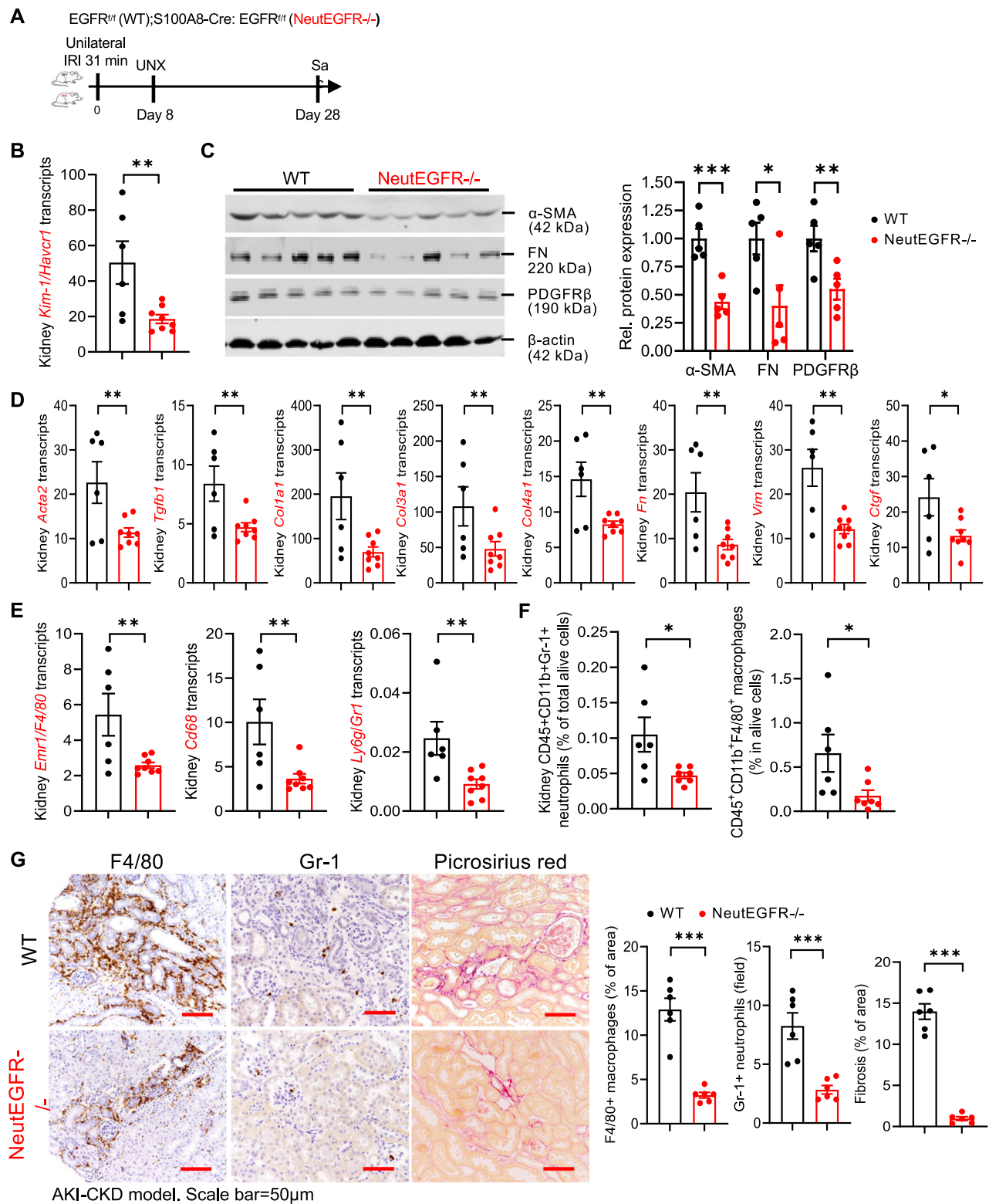
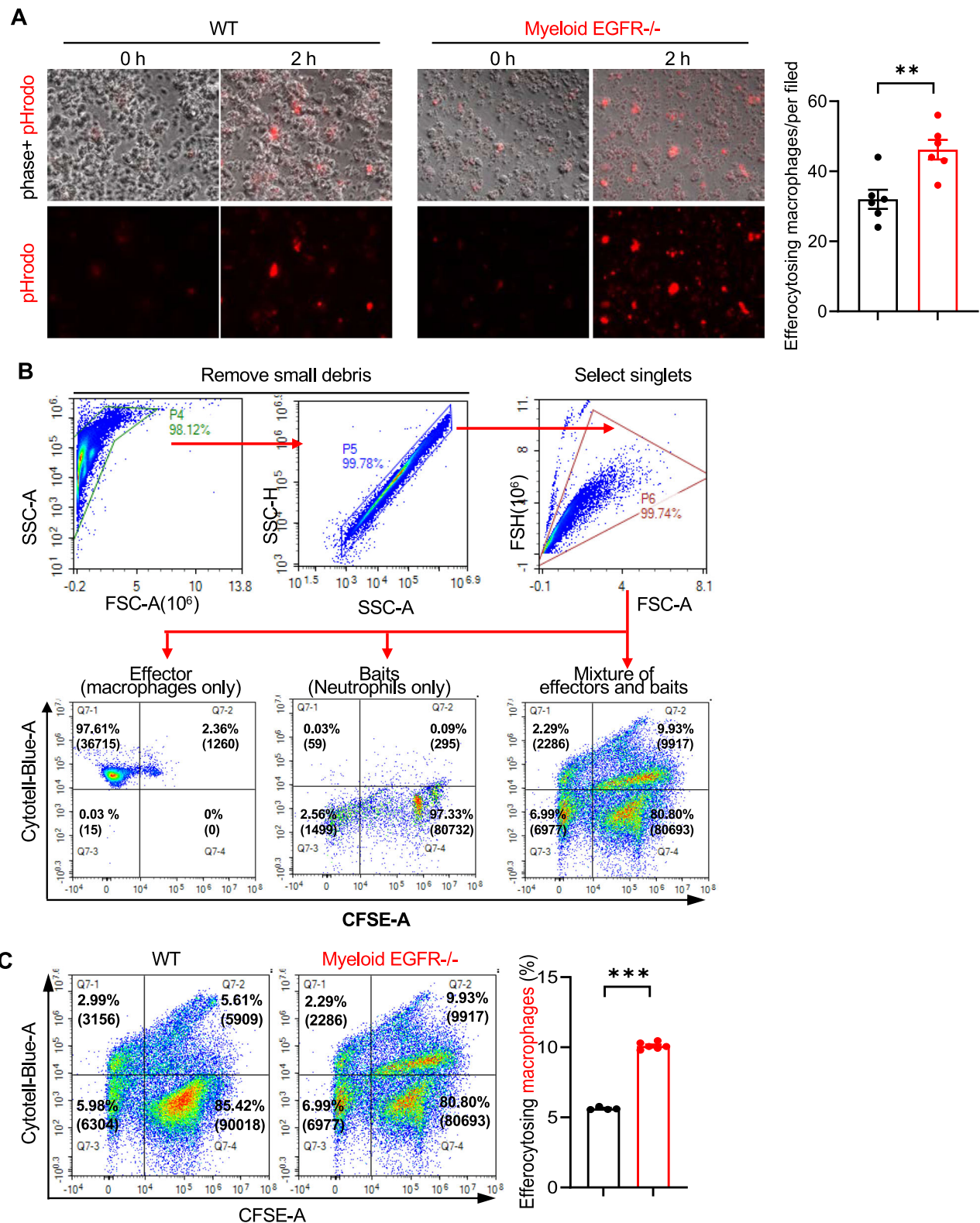


**Fig. 5 | Selective EGFR deletion in neutrophils attenuated development of kidney fibrosis after ischemia injury.** **A** Schematic of experimental protocol. **B–D**, G NeutEGFR<sup>-/-</sup> mouse kidney had less injury, indicated by: **B** lower mRNA levels of *Havcr1/Kim-1* ( $n = 6$  and  $8$ ) and less fibrosis, indicated by: **C** lower protein ( $n = 5$ ) and **D** mRNA levels ( $n = 6$  and  $8$ ) of profibrotic and fibrotic components and **G** decreased

quantitative Picrosirius red staining ( $n = 6$ ). NeutEGFR<sup>-/-</sup> mice had less kidney immune cell infiltration, indicated by: **E** lower mRNA levels of *Emr1/F4/80*, *Cd68* and *Ly6g/Gr1* ( $n = 6$  and  $8$ ), **F** macrophage and neutrophil numbers ( $n = 6$  and  $7$ ), and **G** quantitative F4/80 and Gr-1 staining ( $n = 6$ ). Scale bar =  $50 \mu\text{m}$ . Data are means  $\pm$  SEM, \* $P < 0.05$ , \*\* $P < 0.01$ , \*\*\* $P < 0.001$ , analyzed using 2 tailed Student's  $t$  test.

increased kidney neutrophil apoptosis but fewer kidney neutrophils as determined by flow cytometry (Fig. 9A) and cleaved caspase-9 colocalization in neutrophils (Fig. 9B), less kidney injury as indicated by lower BUN (Fig. 9C) and kidney injury score (Fig. 9D) as well as lower NGAL

mRNA expression and expression of proinflammatory cytokines (Supplementary Fig. S20A–C). However, the Mcl-1 inhibitor had no apparent effect on neutrophil EGFR expression in vivo (Supplementary Fig. S20C). The Mcl-1 inhibitor also increased apoptosis of WT bone



marrow derived neutrophils as indicated by cleaved caspase-3 flow cytometry (Fig. 9E).

#### Mcl-1 inhibition ameliorated ischemic kidney injury

As Mcl-1 inhibition leads to increased neutrophil apoptosis, WT mice with ischemic injury (35-minutes bilateral pedicle clamping to increase survival) were treated with vehicle or an Mcl-1 inhibitor, S63845, daily for 6 days, beginning six hours after initial ischemic

injury. Mice were sacrificed 3 weeks after the ischemic injury (Fig. 10A). Mcl-1 inhibition led to accelerated functional recovery (Fig. 10B), relative preservation of glomerular filtration rate (Supplementary Fig. S10C), and less kidney fibrosis (S10 D-F). To validate the specificity of S63845's ability to inhibit Mcl-1 activity, we generated Mcl-1 hypomorphic HEK293 cell lines. We treated both WT and hypomorphic cell lines with S63845 and determined that the ability of S63845 to inhibit WT HEK293 cell proliferation was



**Fig. 6 | EGFR deletion in myeloid cells increased kidney macrophage efferocytosis ability.** Kidney macrophages were isolated with F4/80 microbeads from myeloid EGFR<sup>-/-</sup> mice and WT mice 2 days after bilateral 35-min renal pedicle clamping. Bone marrow neutrophils were isolated from WT mice with Ly6G microbeads. Myeloid EGFR<sup>-/-</sup> mouse kidney macrophages had increased ability to clear apoptotic neutrophils as indicated by: **A** Ex vivo pHrodo Red real-time efferocytosis assay with apoptotic bone marrow neutrophils ( $n = 6$ ). **B** The full gating strategies for the flow cytometry to evaluate kidney macrophage efferocytosis. The effector kidney macrophages were isolated from WT, myeloid EGFR<sup>-/-</sup> and NeutEGFR<sup>-/-</sup> mice 2 days after ischemic injury using anti-F4/80 microbeads and stained with CytoTell<sup>TM</sup> Blue dye. The bait bone marrow neutrophils were isolated from WT mice using anti-ly6G microbeads and stained with CFSE dye and apoptosis

was induced by staurosporine. The effector cells alone and bait cells alone or a mixture of effectors and baits at a ratio of 1:4 were incubated overnight before processing for flow cytometry. For flow cytometry analysis strategy, first small debris were removed, and singlets selected. Cells were gated on CytoTell<sup>TM</sup>blue positivity and CFSE positivity with macrophages only in the reaction or neutrophils only in reaction as controls. When both CFSE-labeled apoptotic neutrophils and CytoTell<sup>TM</sup>blue-labeled macrophages were both in the reaction, CFSE and CytoTell<sup>TM</sup>blue double positivity represented macrophages with engulfed apoptotic neutrophils (expressed as percentage of total events with event counts in parenthesis). **C** EGFR deletion in myeloid cells increased kidney macrophage efferocytosis ability ( $n = 4$  and 6). Data are means  $\pm$  SEM, \*\* $P < 0.01$ , \*\*\* $P < 0.001$ , analyzed using 2 tailed Student's  $t$  test.

abolished in Mcl-1 hypomorphic HEK293 cells (Supplementary Fig. S21).

## Discussion

We and others have defined an important role for myeloid-derived cells in propagation of acute kidney injury and in the development of chronic renal damage<sup>13,32</sup>. EGFR and its ligands are expressed in a variety of cell types, including cells of myeloid origin. EGFR activation mediates chemotaxis in monocytes and proliferation in macrophages in vitro<sup>17</sup>, but the role of renal myeloid cell EGFR and its ligands in response to acute kidney injury has not been previously studied. The current studies elucidated important roles for EGFR in different myeloid cell types in response to acute kidney injury. Macrophages with EGFR deletion exhibited increased efferocytotic capacity and a pro-resolving, anti-inflammatory phenotype. In addition to elucidating an important role for EGFR expression in macrophages, the current studies demonstrated that EGFR expression and activation in kidney neutrophils play an essential role in extending their life span in kidney injury. Although there were no differences in initial infiltration of neutrophils, deletion of EGFR in neutrophils promoted kidney neutrophil apoptosis, accelerated recovery from acute ischemic injury and reduced subsequent development of tubulointerstitial fibrosis. Although the increased cleaved caspase 9 as well as cleaved caspase 3 in kidneys with selective deletion of neutrophil EGFR indicated increased apoptosis per se, we also recognize that some neutrophils may have undergone other types of programmed cell death.

Expression of EGFR in kidney epithelial cells has been shown to be involved in initial recovery from acute kidney injury and also to mediate development of tubulointerstitial fibrosis<sup>5–11</sup>. Previous studies have indicated that inhibition of EGFR tyrosine kinase activity, either with the tyrosine kinase inhibitor, or in mice with genetic inhibition of intrinsic EGFR kinase activity (*Waved 2* mice) had delayed recovery from ischemic injury<sup>5,9,33</sup>, suggesting that an active epithelial EGFR is necessary for the initial functional recovery. However, the fact that in both *Waved 2* mice and erlotinib administration, subsequent kidney fibrosis was delayed is consistent with important roles for both epithelial and myeloid EGFR.

We have previously reported that macrophage EGFR deletion reduced adipose tissue inflammation and insulin resistance in mice fed a high fat diet<sup>22</sup>. In the current studies, macrophages with selective EGFR deletion isolated from kidneys after ischemic injury had decreased expression of proinflammatory cytokines and increased expression of macrophage markers of an anti-inflammatory, pro-resolving phenotype. Results of the current scRNAseq studies are consistent with initial infiltration of proinflammatory macrophages in response to ischemic kidney injury and also determined that with myeloid EGFR deletion, there was a relative increase in proliferation and differentiation of resident kidney macrophages to a non-inflammatory, pro-resolution phenotype and a relative decrease in pro-inflammatory and profibrotic infiltrating macrophage phenotypes. Whether there was also a phenotypic switch of the infiltrating

macrophages to a pro-resolution phenotype could not be determined in the current studies.

Neutrophils are normally short-lived, but their half-life can increase in inflammatory conditions<sup>34</sup>. Following tissue infiltration, neutrophils can die by apoptosis, ferroptosis, necroptosis, pyroptosis or NETosis. With the exception of apoptosis, these other modes of neutrophil death are in some way involved in promoting inflammation and tissue injury. If there is effective clearance, apoptotic neutrophils do not release internal constituents that can serve as DAMPs to induce a continued inflammatory state. Rather, the apoptotic neutrophils induce “find me” signals (ATP, UTP, lysophosphatidylcholine and sphingosine-1-phosphate) and “eat me” signals (phosphatidylserine and lysophosphatidylserine) that promote their effective phagocytosis.

Rahman et al. used a kinase scan to examine neutrophils undergoing apoptosis in vitro and found that there was inhibition of activation of EGFR and ErbB2<sup>35</sup>. They determined that ErbB inhibitors could increase neutrophil apoptosis even with simultaneous administration of a cAMP analog or GM-CSF, both of which are known to promote neutrophil viability. The present studies indicated that following ischemic kidney injury, there was significantly more early apoptosis of neutrophils in vivo with either selective neutrophil EGFR deletion or pharmacologic EGFR kinase inhibition. scRNAseq results confirmed that EGFR deletion increased the percentage of neutrophils expressing apoptosis-promoting genes. Of interest, in wild type mice, EGFR expression and activation in infiltrating neutrophils was low at two hours following release of the vascular clamp but increased more than 6 fold by 16 h. Furthermore, although there was minimal p-EGFR in infiltrated neutrophils 2 h after ischemic injury, it increased more than 15 fold by 16 h, suggesting that the milieu of the injured kidney was the source of the increased receptor activation. Neutrophil apoptosis with EGFR deletion also increased early after ischemic injury, with a similar pattern seen with administration of the EGFR receptor tyrosine kinase inhibitor, erlotinib.

Mcl-1, a member of the Bcl-2 family, is a primary mediator of neutrophil survival. Unlike many other cell types, neutrophils have minimal expression of other antiapoptotic Bcl-2 family proteins except Bcl-xl<sup>36</sup>. However, Bcl-xl is not essential in preventing neutrophil apoptosis, since deletion of Mcl-1 alone will induce neutrophil apoptosis<sup>37</sup>. Mcl-1 has a short mRNA half-life and a protein half-life of only 3 h due to proteasomal degradation, which is unique among Bcl-2 family members. Mcl-1 sequesters proapoptotic Bcl-2 family members, Bax and Bak, and when there is decreased expression or increased degradation of Mcl-1, these factors are released from their inhibitory state and damage the mitochondrial membrane to release cytochrome c and promote apoptosis. In the current studies, the mRNA levels of all proapoptotic Bcl-2 family members were not different in neutrophils between wild type and EGFR deficient neutrophils. In contrast, selective neutrophil deletion of EGFR inhibited neutrophil Mcl-1 expression after ischemic injury, while immunoreactive Mcl-1 continued to be detected in wild type neutrophils up to 3 days after kidney injury. In addition, neutrophil Mcl-1 mRNA was significantly decreased with neutrophil EGFR deletion while EGF administration increased Mcl-1

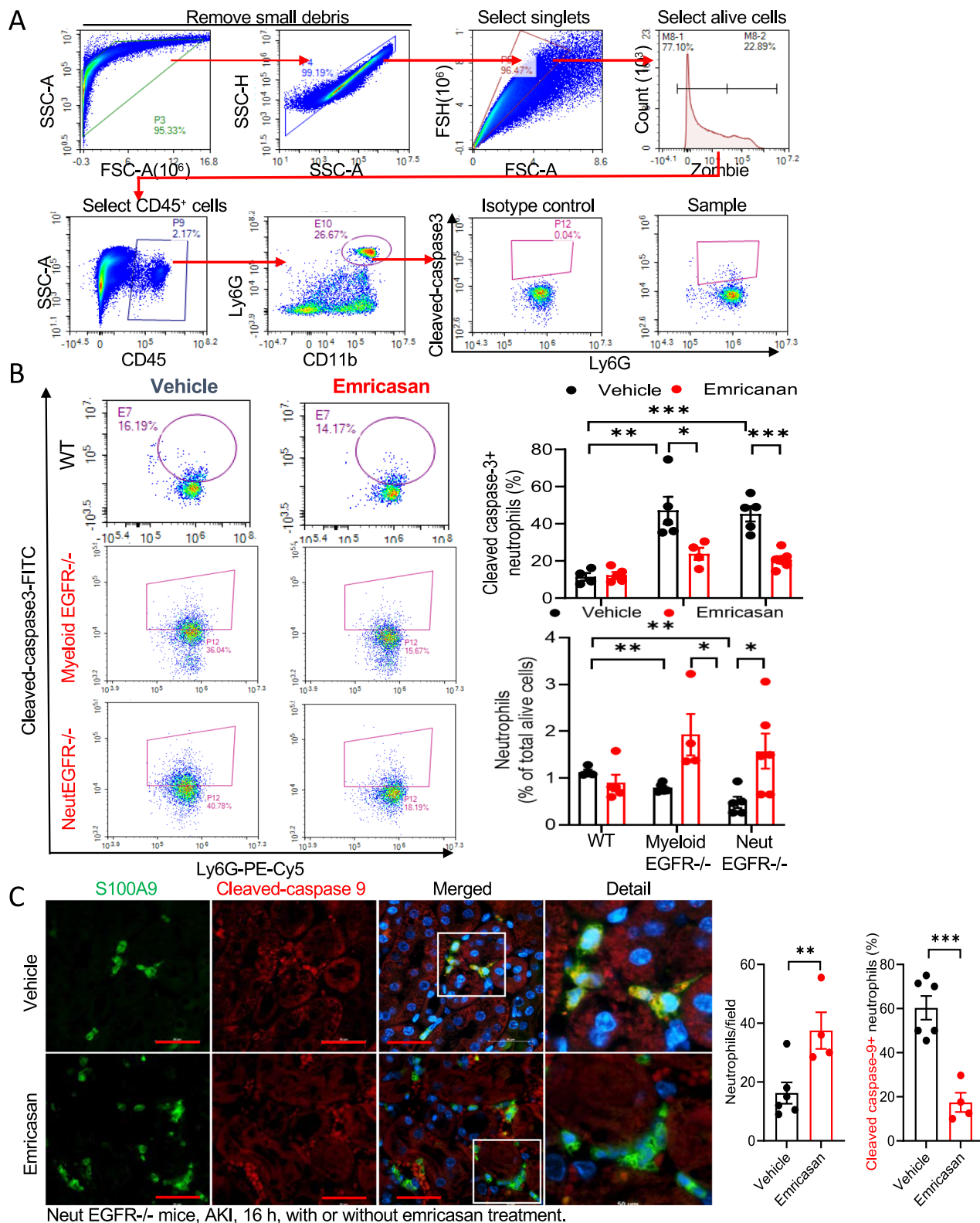


**Fig. 7 | Selective neutrophil EGFR deletion increased neutrophil apoptosis.**

**A** Gating strategy for flow cytometry analysis of cleaved caspase 3 positive apoptotic neutrophils in kidney. **B** WT, myeloid EGFR<sup>-/-</sup>, and NeutEGFR<sup>-/-</sup> mice underwent IRI-UNX for 16 h with or without treatment with emricasan, a pan-caspase inhibitor. Flow cytometry analysis of cleaved caspase 3 indicated that the percentage of kidney apoptotic neutrophils was significantly higher in both myeloid EGFR<sup>-/-</sup> mice ( $n = 4$  and 5) and NeutEGFR<sup>-/-</sup> mice ( $n = 5$  and 6) compared to their corresponding WT mice ( $n = 4$  and 5). Emricasan treatment led to an increased

number of kidney neutrophils due to inhibition of neutrophil apoptosis in both myeloid EGFR<sup>-/-</sup> and NeutEGFR<sup>-/-</sup> mice. **C** Cleaved caspase-9 and S100A9 co-staining indicated that emricasan treatment led to increased numbers of kidney neutrophils and decreased percentage of neutrophil apoptosis in NeutEGFR<sup>-/-</sup> mice. ( $n = 4$  and 6). Scale bar = 50  $\mu$ m for all. Data are means  $\pm$  SEM, \* $P < 0.05$ , \*\* $P < 0.01$ , \*\*\* $P < 0.001$ , analyzed using 2-way ANOVA followed by Bonferroni's post hoc test for (B), and 2 tailed Student's  $t$  test for (C).

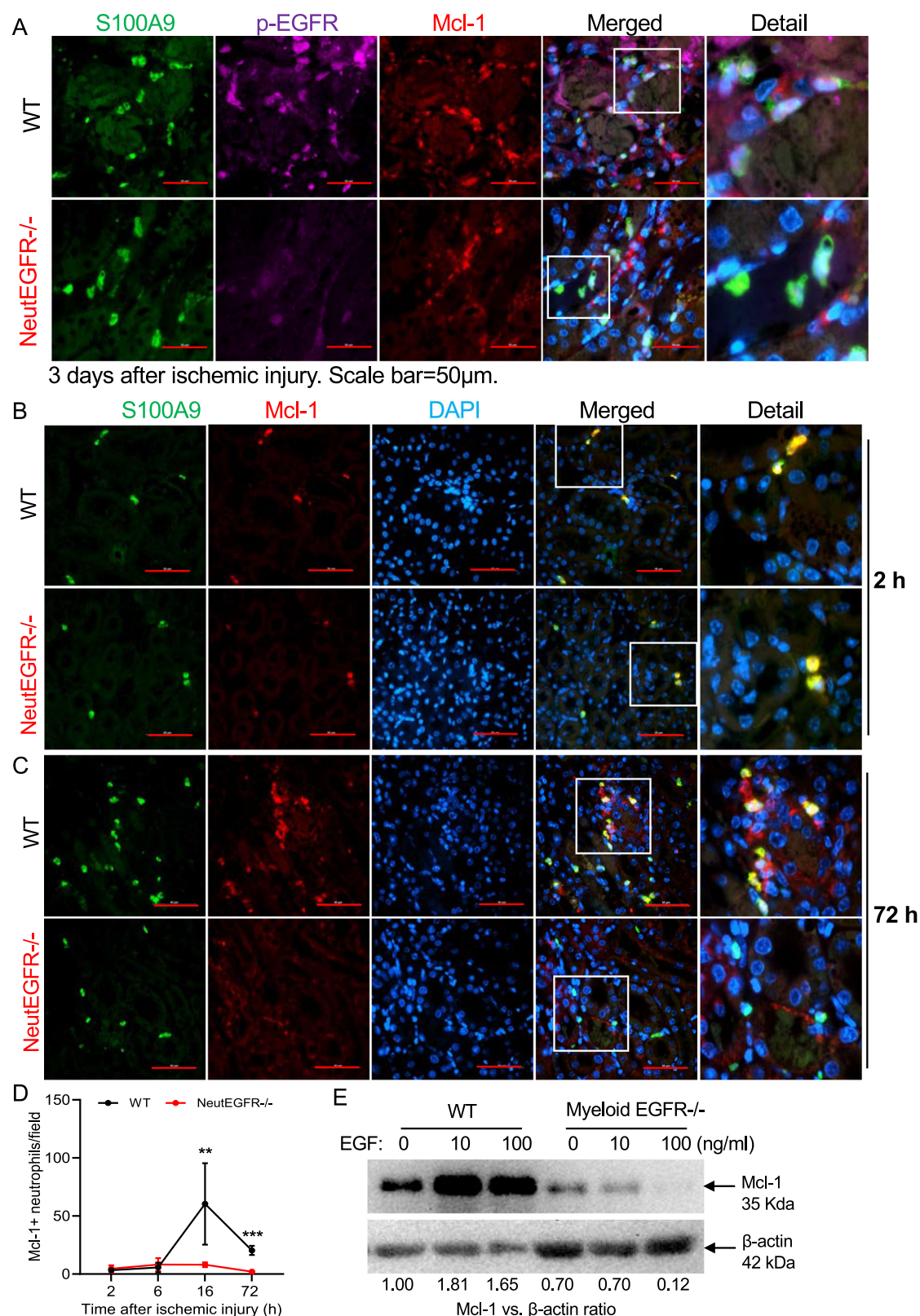


**Fig. 8 | EGFR signaling promoted renal neutrophil survival via maintaining antiapoptotic protein Mcl-1 levels after ischemic injury.** NeutEGFR<sup>-/-</sup> and WT mice underwent ischemic injury and were sacrificed at the indicated time points. **A** Three days after ischemic injury, expression of both p-EGFR and Mcl-1 in kidney neutrophils was evident in WT mice but was minimal in NeutEGFR<sup>-/-</sup> mice. **B–D** After ischemic injury, the number of Mcl-1 expressing neutrophils was

comparable between WT and NeutEGFR<sup>-/-</sup> mice at 2 h and 6 h but was markedly lower at 16 and 72 h in NeutEGFR<sup>-/-</sup> mice ( $n = 5-8$ ). **E** In isolated WT bone marrow neutrophils EGF administration for 16 h induced immunoreactive Mcl-1 protein, which was markedly attenuated in EGFR<sup>-/-</sup> bone marrow neutrophils isolated from myeloid EGFR<sup>-/-</sup> mice. Scale bar = 50 μm for all. Data are means  $\pm$  SD, \*\* $P < 0.01$ , \*\*\* $P < 0.001$ , analyzed using 2-way ANOVA followed by Tukey's post hoc test.



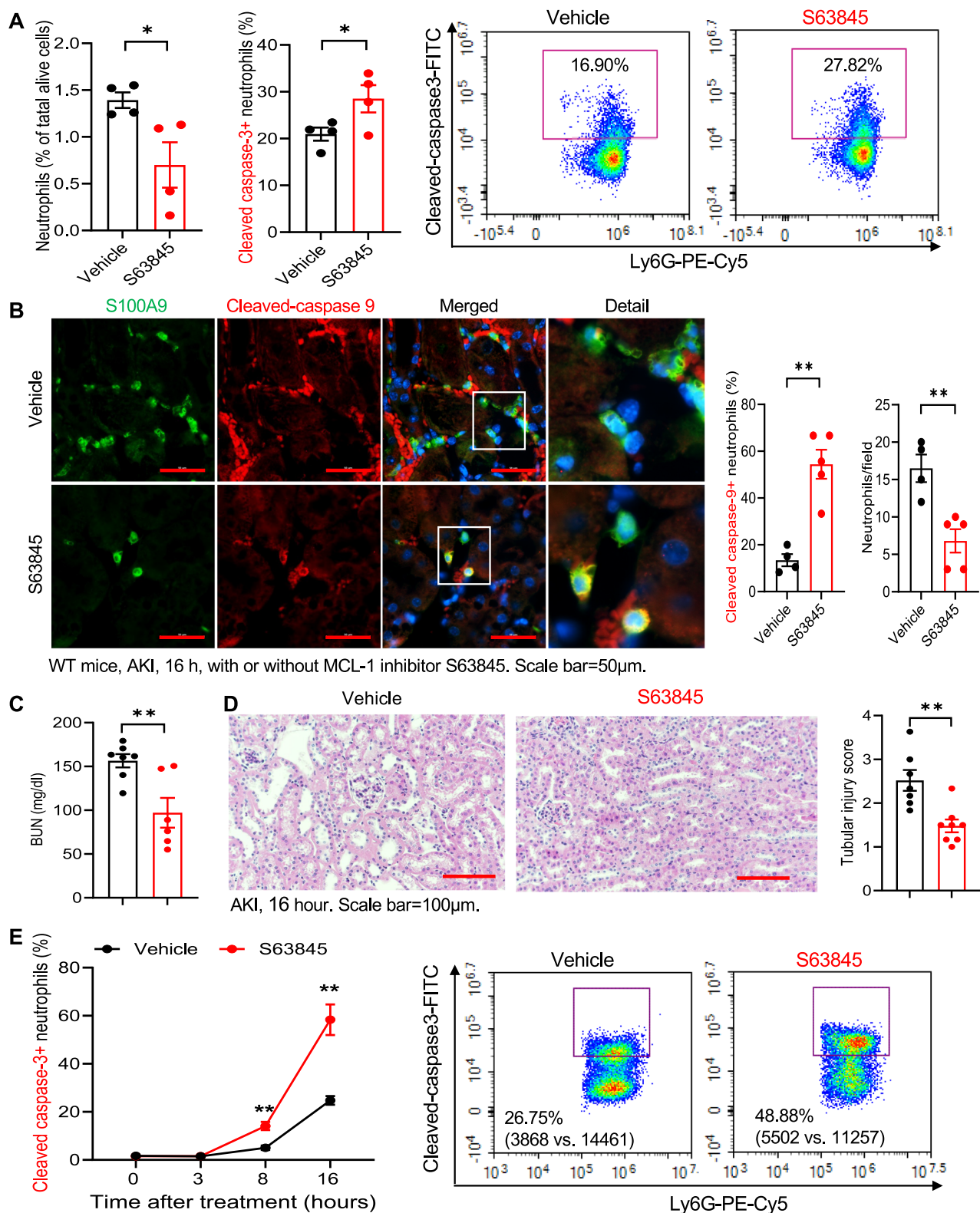


**Fig. 9 | A Mcl-1 inhibitor attenuated ischemic kidney injury.** WT mice were pretreated with the Mcl-1 inhibitor, S63845 and sacrificed 16 h after the ischemic insult. **A–D** S63845 treatment led to decreases in numbers of kidney neutrophils but increases in neutrophil apoptosis evaluated with flow cytometry analysis of cleaved caspase 3 ( $n = 4$ ) (**A**) and cleaved caspase-9 and S100A9 co-staining (4 and 5) (**B**), in association with less injury, indicated by lower BUN ( $n = 6$  and 7) (**C**) and a lower tubular injury score ( $n = 7$  and 8) (**D**). **E** Mcl-1 inhibition with S63845 led to

increased ex vivo bone marrow neutrophil apoptosis determined by cleaved caspase-3 flow cytometric analysis ( $n = 4$ ). Of note, cleaved caspase-3 neutrophil counts vs. total neutrophil counts are presented in parenthesis. Scale bar: 50  $\mu\text{m}$  for (**B**) and 100  $\mu\text{m}$  for (**D**). Data are means  $\pm$  SEM, \* $P < 0.05$ , \*\* $P < 0.01$ , analyzed using 2 tailed Student's  $t$  test for (**A–D**); 2-way ANOVA followed by Tukey's post hoc test for (**E**).

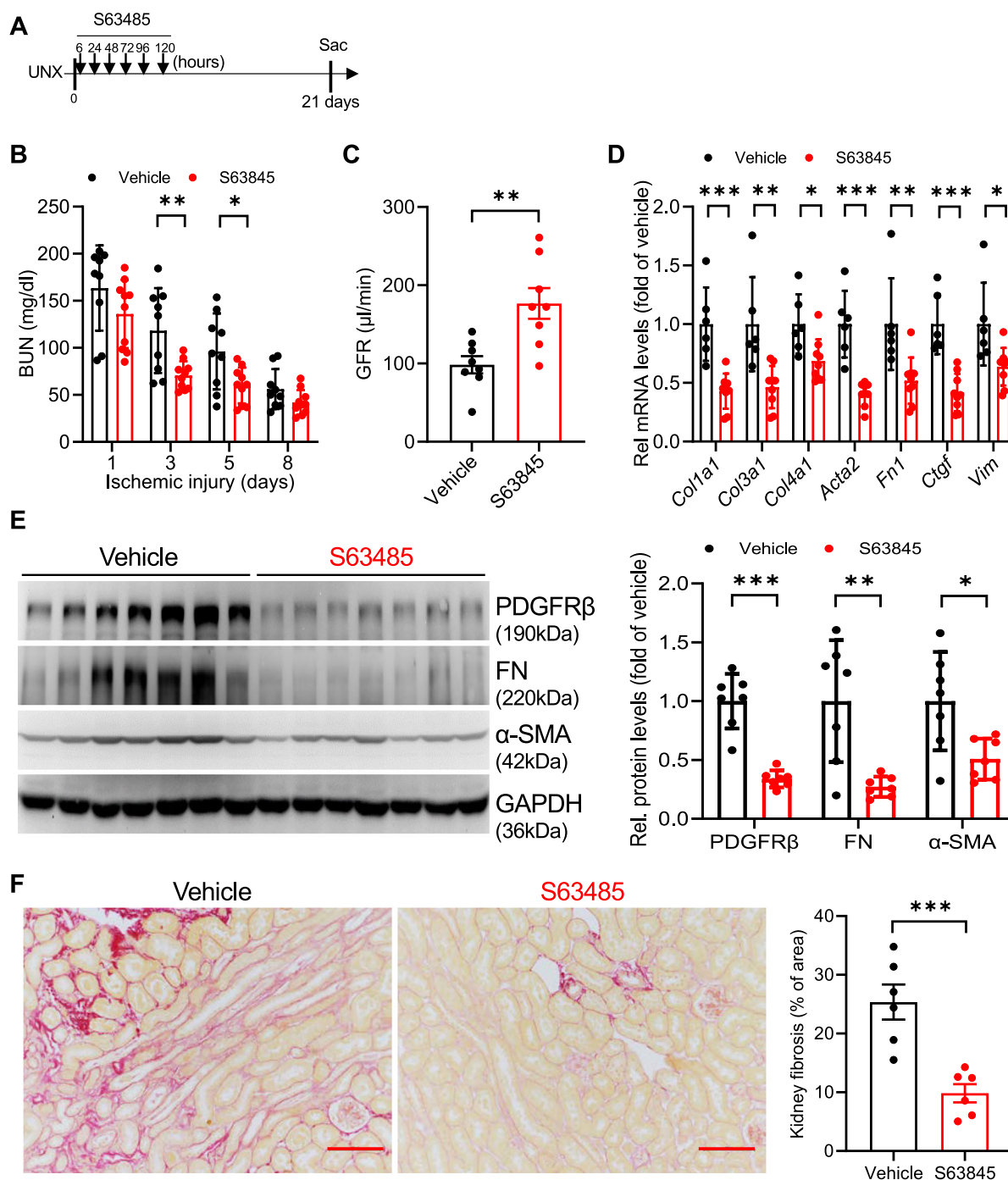


**Fig. 10 | Mcl-1 inhibition accelerated functional recovery from ischemic injury with less post-ischemia fibrosis.** **A** Male C57BL/6 (8 weeks old) mice underwent ischemic injury (renal pedicle clamping, 35 min, both kidneys, Bi-IRI), and the Mcl-1 inhibitor (S63845) was given 6 h later and daily for the next 5 days via intravenous injection at a dose of 5 mg/kg. The mice were sacrificed 3 weeks later. Mcl-1 inhibition accelerated functional recovery, indicated by: **B** rapid BUN decline ( $n = 9$  and

10), **C** preserved GFR ( $n = 8$ ) and attenuation of the development of kidney fibrosis, indicated by: **D** lower mRNA levels ( $n = 6$  and 9) and **E** protein levels ( $n = 7$ ) of profibrotic and fibrotic components as well as **F** quantitative Picrosirius red staining ( $n = 6$ ) (**F**). Scale bar=100  $\mu$ m. Data are means  $\pm$  SEM, \* $P < 0.05$ , \*\* $P < 0.01$ , \*\*\* $P < 0.001$ , analyzed using 2 tailed Student's  $t$  test for all.

protein in bone marrow derived cells, indicating that EGFR activation can increase Mcl-1 transcription and expression. A selective Mcl-1 inhibitor also increased neutrophil apoptosis both in vivo and in vivo, decreased kidney neutrophils and reduced BUN after ischemic injury. These findings further support the conclusion that neutrophil apoptosis mediated by neutrophil EGFR deletion decreases the severity of post-ischemic kidney injury and suggest that the persistent EGFR activation seen in wild type neutrophils in the damaged kidney may be

an important contributing factor to increase neutrophil half-life in inflammatory conditions<sup>34</sup>.

Macrophages are the major cell type mediating neutrophil efferocytosis, which increases the anti-inflammatory phenotype of the macrophages<sup>38,39</sup>. Effective efferocytosis of apoptotic neutrophils is important in the resolution of an acute inflammatory injury both by promoting the polarization of tissue macrophages to a pro-resolution phenotype and by preventing release of further proinflammatory cell

contents. Therefore, these studies identify coordinated and complementary detrimental effects in acute kidney injury of EGFR expression in different cells of myeloid origin, since the dual actions of increased apoptosis of neutrophils and increased phagocytic ability of macrophages with myeloid EGFR deletion serve to increase neutrophil efferocytosis, promoting a proresolving macrophage phenotype, reducing an inflammatory milieu that would promote increased neutrophil half-life and inhibiting secondary necrosis of apoptotic neutrophils to prevent release of DAMPs that could lead to further inflammation and injury. Although we did observe increased efferocytosis in MyeloidEGFR<sup>-/-</sup> mice, we did not see a comparable increased efferocytosis in NeutEGFR<sup>-/-</sup> mice, which we attribute to the decreased macrophage efferocytosis capability in macrophages with intact EGFR activity.

## Methods

### Sex as a biological variable

To delete EGFR murine expression, we utilized CD11b-Cre mice. The transgene integration is on the Y chromosome so only male mice could be used.

### Animals

All animal experiments were performed in accordance with the guidelines of the Institutional Animal Care and Use Committee of Vanderbilt University. EGFR floxed (EGFR<sup>fl/fl</sup>) mice were generated by flanking exon 3 of the EGFR gene with two LoxP sites, as described previously<sup>40</sup>. CD11b-Cre mice with transgene integration in the Y chromosome were generated in Dr. Vacher's laboratory<sup>41</sup>. MRP8-Cre/S100A8-Cre mice (Strain#: 021614, C57BL/6J) (S100A8-Cre) were purchased from The Jackson Laboratory. Myeloid EGFR deletion (CD11b-Cre: EGFR<sup>fl/fl</sup>, myeloid EGFR<sup>-/-</sup>) and neutrophil EGFR deletion (S100A8-Cre: EGFR<sup>fl/fl</sup>, Neut EGFR<sup>-/-</sup>) and corresponding wild type (EGFR<sup>fl/fl</sup>) mice were used. 8–12 week old male mice were used in the experiments and were genotyped with PCR before and after the study was completed. The primers used for genotyping in the current studies are listed in Supplementary Table S1. Animals were euthanized with CO<sub>2</sub>, followed by cervical dislocation.

### Kidney injury models

For the ischemic acute kidney injury (AKI) model, the mice were anesthetized with isoflurane with a Precision vaporizer for all surgeries and before sacrifice. Unless otherwise indicated, ischemia-reperfusion-induced AKI was carried out as previously described<sup>42</sup>. Briefly, the animals were uninephrectomized, immediately followed by unilateral ischemia-reperfusion with kidney pedicle clamping for 28.5 min. An AKI-CKD model was performed according to methods described by Skrypnik et al. Following anesthesia, the left renal pedicle was clamped for 35 min, leaving the right kidney intact. 8 days later, the right kidney was removed. 20 days later the animals were sacrificed and the remaining left kidney was studied<sup>28</sup>.

### In vivo drug treatment

8–12 week old wild-type C57BL/6 mice from Jackson Laboratory were used for in vivo drug experiments. Erlotinib was prepared in PBS and was administered at 80 mg/kg/day via gastric gavage for two days before surgery. Drug and vehicle pretreated wild-type C57BL/6 mice underwent bilateral ischemia-reperfusion with renal pedicle clamping for 35 min.

The Mcl-1 inhibitor S63845 (MedChemExpress) was formulated and protected from light in 2% Vitamin E/TPGS (Sigma) in NaCl 0.9% (w/v) and was delivered to wild-type C57BL/6 mice by retro-orbital injection for 2 days prior to, and on the day of surgery for acute experiments. For therapeutic experiments, S63845 was given at a dose of 5 mg/kg/day daily from 6 h after initial injury to day 7 via intravenous injection, and the mice were sacrificed at 21 days.

### Antibodies and reagents

The information of all antibodies used is listed in Supplementary Table S2.

### Isolation and polarization of bone marrow derived monocytes (BMDMs)

Mice were anesthetized with isoflurane and sacrificed by cervical dislocation. Femurs, tibias, and humeri were dissected, and the shafts were flushed using a syringe and a 26-gauge needle with RPMI1640 supplemented with 100 U/ml penicillin, 100 µg/ml streptomycin, 10 U/ml heparin, and 0.2% fetal bone serum (FBS). The cell suspension was passed through a 40-µm strainer, centrifuged, and the pellets were resuspended in 3 ml red blood cell lysis buffer and incubated for 10 min on ice. After centrifugation, the pellets were resuspended with 10 ml Dulbecco's PBS containing 0.5% FBS, followed by monocyte isolation using a monocyte isolation kit for mice (Miltenyi Biotec, 130-100-629).

### Quantitative immunofluorescence/immunohistochemistry staining

Kidney tissue was immersed in fixative containing 3.7% formaldehyde, 10 mM sodium m-periodate, 40 mM phosphate buffer, and 1% acetic acid. The tissue was dehydrated through a graded series of ethanols, embedded in paraffin, sectioned (5 µm), and mounted on glass slides. Antigen retrieval in the deparaffinized sections was performed with citrate buffer by microwave heat for 10 min and the slides were then blocked with 10% normal donkey serum for 1 h at RT followed by incubation with primary antibodies overnight at 4 °C. For immunofluorescence staining, the sections were incubated in two rounds of staining overnight at 4 °C. Anti-rabbit or mouse IgG-HRP were used as secondary antibodies (Cell Signaling Technology). Each round was followed by tyramide signal amplification with the appropriate fluorophore (Alexa Fluor 488 tyramide, Alexa Fluor 647 tyramide or Alexa Fluor 555 tyramide, Tyramide SuperBoost Kit with Alexa Fluor Tyramides, Invitrogen) according to its manufacturer's protocols. DAPI was used as a nuclear stain. Sections were viewed and imaged with a Nikon TE300 fluorescence microscope and spot-cam digital camera (Diagnostic Instruments), followed by quantification of cells/field using Image J software (NIH, Bethesda, MD). IOD were calculated in more than 30 fields per mouse or 10 fields per cell slide and expressed as arbitrary units or percentage per field by two independent investigators.

### Isolation of kidney macrophages and neutrophils

Kidney macrophages and neutrophils in kidney single-cell suspensions were enriched using anti-F4/80 microbeads (130-110-443; Miltenyi Biotec) and anti-Ly6G microbeads (130-120-337; Miltenyi Biotec), respectively, and MACS columns (130-110-443, Miltenyi Biotec) following the manufacturer's protocol<sup>43</sup>.

### Engineered MCL1 deletion cell line

The human MCL1 gene sequence was obtained from the UCSC Genome Browser (GRCh38/hg38). Three guide RNA sequences (guide RNA1: 5'-ATCGGACTCAACCTCTACTG-3'; guide RNA2: 5'-GGTAATAACACCAGTACGGA-3'; guide RNA3: 5'-ACTTTTGCTACGGAGAAGG-3') were selected from exon1 using the predesigned Alt-R CRISPR-Cas9 guide RNA tool from Integrated DNA Technologies. Guide RNA sequences were cloned downstream of the U6 promoter of pX330-U6-Chimeric\_BB-CBh-hSpCas9 (Addgene #42230). The GFP-Puro sequence with flanking MCL1 sequences was amplified with Q5 polymerase and purified with a Gel and PCR Clean-up kit (Macherey-Nagel). HEK293 cells were transfected with plasmid containing the MCL1 guide RNA sequence and hspCas9 and GFP-Puro amplicons using lipofectamine LTX according to the manufacturer. Transfected HEK293 cells were selected with 3 mg/ml of puromycin for three weeks. Puromycin



selected cells were collected, and genomic DNA was prepared with the DNeasy Blood and Tissue Kit (Qiagen). Genomic DNA fragments covering guide RNA sequences were amplified with primers MCL1 F: 5'-TCTTCCCCAGTTTCTCAGCCAGG-3' and MCL1 R: 5'-CGAGAGATAATCTCCAGCGACTGC-3' and purified with the Gel and PCR Clean-up kit. Amplicons were sequenced with Nanopore next generation sequencing. Sequenced data was mapped to MCL1 gene using BWA-MEM and viewed using the Integrated Genome Browser. MCL1 knockout efficiencies were calculated for each guide RNA. The Indel rate for guide RNA1 was 73.1%, guide RNA2, 67.9%, guide RNA3 69.8%. These cells were subsequently used for Western blot and stimulation experiments.

### Flow cytometry analysis

Kidney single cell suspensions were prepared according to previous reports<sup>44</sup>. Cells were stained with Zombie Violet™ (Biolegend, Cat# 423114) for 10 min at RT and then incubated in 2.5 µg/ml Fc blocking solution, centrifuged (300 × g, 10 min, 4 °C) and resuspended with FACS buffer. Cells were stained for 60 min at 4 °C with fluorescent conjugated antibodies against different cell marker antigens (Supplementary Table S2) or isotype control. A total of 50,000–100,000 cells were acquired by scanning using NovoCyte Quanteon Flow Cytometer Systems. Cell debris and dead cells were excluded from the analysis based on scatter signals and use of Zombie Violet™ Fixable Viability. For determination of blood neutrophils and monocytes, blood was collected in heparinized tubes, erythrocytes were lysed and the remaining cells were prepared and analyzed by FACS as indicated above.

For evaluation of monocyte infiltration into renal tissue, 100 µl of solution containing 10<sup>6</sup> PKH26-labeled WT BMDMs (red, PKH26GL, Sigma-Aldrich) and 10<sup>6</sup> PKH67-labeled EGFR<sup>-/-</sup> BMDMs (from CD11bCre EGFR<sup>-/-</sup> mice) (green, PKH67GL, Sigma-Aldrich) were injected retro-orbitally into either WT or CD11bCre EGFR<sup>-/-</sup> mice.

### Evaluation of macrophage ability to clear apoptotic neutrophils

**Ex vivo real-time efferocytosis assay.** Bone marrow neutrophils were isolated from WT mice using Ly6G microbeads, cultured in serum-free DMEM with pHrodo Red at 5 µg/ml for 30 min at 37 °C, washed with 10% FBS DMEM to remove unbound dye, and then incubated with staurosporine (1: 1000) in 10% FBS DMEM for 2 h to induce apoptosis. After two washes with 10% FBS DMEM medium, the cells were resuspended in phenol red free 10% FBS medium. Kidney macrophages were isolated by F4/80 microbeads from WT mice and myeloid EGFR<sup>-/-</sup> mice 2 days after ischemic injury (bilateral renal pedicle clamping, 35 min) and seeded in a 24-well plate in phenol red free 10% DMEM medium for 30 min. pHrodo Red labeled apoptotic neutrophils were added at a 4:1 ratio. Photos were taken on the same spots at 0 and 2 h. pHrodo+ macrophages were counted.

**Efferocytosis assay with flow cytometry.** An efferocytosis assay kit (No.601770, Cayman Chemical) was used to evaluate the effect of myeloid EGFR deletion on kidney macrophage efferocytosis following the manufacturer's protocol. WT bone marrow neutrophils isolated as above were stained with CFSE and apoptosis was induced by staurosporine. Kidney macrophages isolated from WT mice and myeloid EGFR<sup>-/-</sup> mice were stained with CytoTell blue. A mixture of CFSE labeled apoptotic neutrophils and CytoTell blue labeled renal macrophages (4:1) was plated onto 6-well plates (3 × 10<sup>5</sup> cells/well) and cultured for 16 h at 37 °C. For flow cytometry analysis of efferocytosis, cells were gated on CytoTell blue positivity before counting the CFSE positive cells.

For analysis of annexin V positivity with flow cytometry, cells were stained with annexin V conjugate-FITC dye (1:20, ThermoFisher, A13199) for 15 min at RT followed by flow cytometry.

**Bone marrow neutrophil apoptosis study.** Bone marrow neutrophils from C57BL/6J WT mice were cultured in RPMI 1640 medium containing 10% FBS. The cells were treated with 10 µM Mcl-1 inhibitor (S63845, Selleckchem) for 0, 3, and 6 h followed by staining with Zombie Violet™, Ly6G and Annexin V for analysis by flow cytometry.

**Immunoblotting analysis.** Whole kidney tissue or isolated bone marrow cells was homogenized with lysis buffer containing 10 mmol/l Tris-HCl (pH 7.4), 50 mmol/l NaCl, 2 mmol/l EGTA, 2 mmol/l EDTA, 0.5% Nonidet P-40, 0.1% SDS, 100 µmol/l Na3VO4, 100 mmol/l NaF, 0.5% sodium deoxycholate, 10 mmol/l sodium pyrophosphate, 1 mmol/l PMSF, 10 µg/ml aprotinin, and 10 µg/ml leupeptin and centrifuged at 15,000 × g for 20 min at 4 °C. The BCA protein assay kit (Thermo Scientific) was used to measure the protein concentration. Immunoblotting was performed as previously described<sup>45,46</sup> and quantitated with Image J software.

**Quantitative PCR.** Total RNAs from kidneys or cells were isolated using Trizol® reagent (Invitrogen). SuperScript IV First-Strand Synthesis System kit (Invitrogen) was used to synthesize cDNA from equal amounts of total RNA from each sample. Quantitative RT-PCR was performed using TaqMan real-time PCR (7900HT, Applied Biosystems). The Master Mix and all gene probes were also from Applied Biosystems. The primers used for qPCR in the experiments are presented as Supplementary Table S3. Realtime PCR data were analyzed using the 2-ΔΔCT method to determine the fold difference in expression. Generally, 500 ng mRNA, measured by Nanodrop 2000, was obtained from isolated kidney tissue myeloid cells.

**Histology analysis.** Hematoxylin and eosin (H&E) stained slides were evaluated for tubular injury without knowledge of the identity of the various groups. A semiquantitative evaluation was used to evaluate the degree of tubular injury. Each low power field of tubules on a single section was graded from 0 to 5, with 1, 2, 3, 4 and 5 representing tubular injury, <10, 10–25, 25–50, 50–75, or >75% of the injury area, respectively. Tubular injury includes dilation of the tubules and flattening of the tubular epithelium, tubular casts, fragments of cells or necrotic epithelium in the tubular lumen, loss of brush border, loss of nuclei, and denudation of the basement membrane.

Picrosirius red stain was performed according to the protocol provided by the manufacturer (Sigma, St. Louis, MO, USA).

**Measurement of BUN.** BUN was measured using a Urea Assay Kit (BioAssay Systems, Hayward, CA).

**Single-cell RNA sequencing (scRNA-seq) data processing.** Raw sequencing data were processed following the Chromium's Cell Ranger 3.1.0 pipeline with default parameters. The raw sequencing data (FASTQs files) were aligned to the mouse genome using STAR algorithm. Then gene-barcode matrices containing the barcoded cells and gene expression counts were generated and imported into the R package DropletUtil (version 1.16.0) to identify cells from empty droplets and removal of barcode-swapped pseudo-cells. Seurat (version 4.1.1) R toolkit was used for quality control and subsequent analysis. Unless specified, the default parameters were used for all functions. For quality control, genes that were expressed in more than 10 cells, cells with detected genes between 300 and 7000, mitochondrial gene percentages less than 30%, unique gene counts more than 1000 were kept. In the remaining cells, gene expression matrices were log normalized for each cell by the total expression and multiplied by a scale factor (10,000 by default). Principal component analysis (PCA) for dimensional reduction was performed based on the highly variable genes (top 2000). Clusters were then visualized using the Uniform Manifold Approximation and Projection (UMAP) (ArXiv e-prints 1802.03426, 2018). Cell type identification was performed based on

the expression of known cell markers<sup>25–27</sup>. Differentially expressed genes were identified using “FindAllMarkers” in Seurat.

**Gene set enrichment analysis.** The Gene Ontology (GO) and Kyoto Encyclopedia of Genes and Genomes (KEGG) enrichment analyses were completed using the “clusterProfiler” package (v4.4.4) in R. Biological process and 0.05 *P* value cutoff were chosen. Heatmap indicated each GO term’s significance (–log<sub>10</sub> *P* value). GSEA plot performed using the R package “enrichplot” package (v 1.16.2).

**Pseudotime trajectory analysis.** Pseudotime trajectory analysis was performed using the software of CellRank (v 1.5.1)<sup>47</sup>. CellRank is a toolkit for revealing cell dynamics based on scRNA sequence data and RNA velocity annotation. We set up CellRank’s CytoTRACEKernel to compute a transition matrix based on the CytoTRACE score and visualize the transition matrix via streamlines in the umap embedding.

**Statistical analysis for scRNA-seq analysis.** R software (v4.2.1) was used for all statistical analyses. Data visualization was performed using the R package ggplot2 [v3.4.4]. The heatmap was then plotted by the “pheatmap” package (v1.0.12) in R for visualization. A list of differentially expressed genes of each cell cluster is presented as Supplementary Data S1 and S2.

**Statistical analysis.** Statistical analyses were performed with GraphPad Prism 10 (GraphpadSoftware® Inc., La Jolla, CA, US). Data are presented as the mean ± S.E.M unless indicated in the text. Data were analyzed using 2 tailed Student’s *t* test or two-way ANOVA followed by Tukey’s or Bonferroni’s post hoc tests. A *p* value less than 0.05 was considered significant. For each set of data, at least 4 different animals were examined for each condition. Collection, analysis, and interpretation of data were conducted by at least 2 independent investigators, who were blinded to the study.

**Study approval.** All animal experiments were performed in accordance with the guidelines and with the approval of the Institutional Animal Care and Use Committee of Vanderbilt University.

## Reporting summary

Further information on research design is available in the Nature Portfolio Reporting Summary linked to this article.

## Data availability

The raw data and processed gene expression data in this paper are deposited into the NCBI GEO database:GEO:GSM8146177, GSM8146178, GSM8146179, GSM8146180. Source data are provided with this paper.

## References

- Chen, J.-C. et al. Expression and function of the epidermal growth factor receptor in physiology and disease. *Physiological Rev.* **96**, 1025–1069 (2016).
- Harris, R. C. The epidermal growth factor receptor axis and kidney fibrosis. *Curr. Opin. Nephrol. Hypertens.* **30**, 275–279 (2021).
- Kowski, M. X. Untangling the ErbB signalling network. *Nat. Rev. Mol. Cell Biol.* **2**, 127–137 (2001).
- Schlessinger, J. Ligand-induced, receptor-mediated dimerization and activation of EGF receptor. *Cell* **110**, 669–672 (2002).
- Chen, J., Chen, J. K. & Harris, R. C. Deletion of the epidermal growth factor receptor in renal proximal tubule epithelial cells delays recovery from acute kidney injury. *Kidney Int.* **82**, 45–52 (2012).
- Chen, J. et al. EGFR signaling promotes TGFβ-dependent renal fibrosis. *J. Am. Soc. Nephrol.* **23**, 215–224 (2012).
- Zhang, M.-Z. et al. The role of the epidermal growth factor receptor in gender disparities in kidney injury. *J. Am. Soc. Nephrol.* **30**, 1659–1673 (2019).
- Zhang, M. Z. et al. The Role of the EGF Receptor in Sex Differences in Kidney Injury. *J. Am. Soc. Nephrol.* **30**, 1659–1673 (2019).
- Tang, J. et al. Sustained activation of EGFR triggers renal fibrogenesis after acute kidney injury. *Am. J. Pathol.* **183**, 160–172 (2013).
- Overstreet, J. M. et al. Selective activation of epidermal growth factor receptor in renal proximal tubule induces tubulointerstitial fibrosis. *FASEB J.* **31**, 4407–4421 (2017).
- Cao, S. et al. Epidermal growth factor receptor activation is essential for kidney fibrosis development. *Nat. Commun.* **14**, 7357 (2023).
- Bao, P. Q. et al. Phase II study of gemcitabine and erlotinib as adjuvant therapy for patients with resected pancreatic cancer. *Ann. Surg. Oncol.* **18**, 1122–1129 (2011).
- Zhang, M. Z. et al. CSF-1 signaling mediates recovery from acute kidney injury. *J. Clin. Invest.* **122**, 4519–4532 (2012).
- Harris, R. C. Targeting the ERK pathway reduces liver metastasis of Smad4-inactivated colorectal cancer. *Am. J. Physiol. Ren. Physiol.* **14**, 1059–1067 (2013).
- Harris, R. C. The Role of the Epidermal Growth Factor Receptor in Diabetic Kidney Disease. *Cells* **11**, 3416 (2022).
- Zeng, F., Singh, A. B. & Harris, R. C. The role of the EGF family of ligands and receptors in renal development, physiology and pathophysiology. *Exp. Cell Res.* **315**, 602–610 (2009).
- Lamb, D. J., Modjtahedi, H., Plant, N. J. & Ferns, G. A. EGF mediates monocyte chemotaxis and macrophage proliferation and EGF receptor is expressed in atherosclerotic plaques. *Atherosclerosis* **176**, 21–26 (2004).
- Hardbower, D. M. et al. EGFR regulates macrophage activation and function in bacterial infection. *J. Clin. Invest.* **126**, 3296–3312 (2016).
- Hardbower, D. M. et al. Ornithine decarboxylase regulates M1 macrophage activation and mucosal inflammation via histone modifications. *Proc. Natl Acad. Sci. USA* **114**, E751–E760 (2017).
- Lawrence, S. M., Corriden, R. & Nizet, V. How Neutrophils Meet Their End. *Trends Immunol.* **41**, 531–544 (2020).
- Lewkowicz, P., Tchorzewski, H., Dytnerska, K., Banasik, M. & Lewkowicz, N. Epidermal growth factor enhances TNF-α-induced priming of human neutrophils. *Immunol. Lett.* **96**, 203–210 (2005).
- Cao, S. R. et al. EGFR-mediated activation of adipose tissue macrophages promotes obesity and insulin resistance. *Nat. Commun.* **13**, 4684 (2022).
- Pan Y., et al. Cyclooxygenase-2 in adipose tissue macrophages limits adipose tissue dysfunction in obese mice. *J. Clin. Invest.* **132**, e152391 (2022).
- Huen, S. C. & Cantley, L. G. Macrophages in Renal Injury and Repair. *Annu. Rev. Physiol.* **79**, 449–469 (2017).
- Zimmerman, K. A. et al. Single-Cell RNA Sequencing Identifies Candidate Renal Resident Macrophage Gene Expression Signatures across Species. *J. Am. Soc. Nephrol.* **30**, 767–781 (2019).
- Park, J. et al. Single-cell transcriptomics of the mouse kidney reveals potential cellular targets of kidney disease. *Science* **360**, 758–763 (2018).
- Dhillon, P. et al. The Nuclear Receptor ESRRA Protects from Kidney Disease by Coupling Metabolism and Differentiation. *Cell Metab.* **33**, 379–394.e8 (2021).
- Skrypnik, N. I., Harris, R. C. & de Caestecker, M. P. (2013) Ischemia-reperfusion model of acute kidney injury and post injury fibrosis in mice. *J. Vis. Exp.* **78**, 50495 (2013).
- Moulding, D. A., Quayle, J. A., Hart, C. A. & Edwards, S. W. Mcl-1 expression in human neutrophils: regulation by cytokines and correlation with cell survival. *Blood* **92**, 2495–2502 (1998).
- Ma, G. et al. Overcoming acquired resistance to third-generation EGFR inhibitors by targeting activation of intrinsic apoptotic

- pathway through Mcl-1 inhibition, Bax activation, or both. *Oncogene* **41**, 1691–1700 (2022).
31. Montero, J. et al. Destabilization of NOXA mRNA as a common resistance mechanism to targeted therapies. *Nat. Commun.* **10**, 5157 (2019).
  32. Lee, S. et al. Distinct macrophage phenotypes contribute to kidney injury and repair. *J. Am. Soc. Nephrol.* **22**, 317–326 (2011).
  33. Abdelmageed, M. M., et al. TNF or EGFR inhibition equally block AKI-to-CKD transition: opportunities for etanercept treatment. *Nephrol. Dial. Transplant.* **38**, 1139–1150 (2023).
  34. Summers, C. et al. Neutrophil kinetics in health and disease. *Trends Immunol.* **31**, 318–324 (2010).
  35. Rahman, A. et al. Inhibition of ErbB kinase signalling promotes resolution of neutrophilic inflammation. *Elife*. **8**, e50990 (2019).
  36. Murphy, M. P. & Caraher, E. Mcl-1 is vital for neutrophil survival. *Immunol. Res.* **62**, 225–233 (2015).
  37. Dzhagalov, I., St John, A. & He, Y. W. The antiapoptotic protein Mcl-1 is essential for the survival of neutrophils but not macrophages. *Blood* **109**, 1620–1626 (2007).
  38. Fadok, V. A. et al. Macrophages that have ingested apoptotic cells in vitro inhibit proinflammatory cytokine production through autocrine/paracrine mechanisms involving TGF- $\beta$ , PGE<sub>2</sub>, and PAF. *J. Clin. Invest.* **101**, 890–898 (1998).
  39. Zhang, S. et al. Efferocytosis Fuels Requirements of Fatty Acid Oxidation and the Electron Transport Chain to Polarize Macrophages for Tissue Repair. *Cell Metab.* **29**, 443–456.e5 (2019).
  40. Abe, F. et al. Myeloid-derived suppressor cells in mammary tumor progression in FVB Neu transgenic mice. *Cancer Immunol. Immunother.* **59**, 47–62 (2010).
  41. Ferron, M. & Vacher, J. Targeted expression of Cre recombinase in macrophages and osteoclasts in transgenic mice. *Genesis* **41**, 138–145 (2005).
  42. Pan, Y. et al. Myeloid cyclooxygenase-2/prostaglandin E<sub>2</sub>/E-type prostanoid receptor 4 promotes transcription factor MafB-dependent inflammatory resolution in acute kidney injury. *Kidney Int.* **101**, 79–91 (2022).
  43. Wang, Y. et al. Proximal tubule-derived colony stimulating factor-1 mediates polarization of renal macrophages and dendritic cells, and recovery in acute kidney injury. *Kidney Int.* **88**, 1274–1282 (2015).
  44. Sasaki, K. et al. Deletion of Myeloid Interferon Regulatory Factor 4 (Irf4) in Mouse Model Protects against Kidney Fibrosis after Ischemic Injury by Decreased Macrophage Recruitment and Activation. *J. Am. Soc. Nephrol.* **32**, 1037–1052 (2021).
  45. Zhang, M. Z. et al. Role of epoxyeicosatrienoic acids (EETs) in mediation of dopamine's effects in the kidney. *Am. J. Physiol. Ren. Physiol.* **305**, F1680–F1686 (2013).
  46. Zhang, M. Z. et al. Inhibition of cyclooxygenase-2 in hematopoietic cells results in salt-sensitive hypertension. *J. Clin. Invest.* **125**, 4281–4294 (2015).
  47. Lange, M. et al. CellRank for directed single-cell fate mapping. *Nat. Methods* **19**, 159–170 (2022).
- (R.C.H.), The Vanderbilt Center for Kidney Disease, and Natural Science Foundation of China (No. 81870490) and Shanghai Pujiang Program (22PJ1409300) to Y.P. The Vanderbilt VANTAGE NGS sequencing core provided technical assistance for this work. VANTAGE is supported in part by CTSA Grant (5UL1 RR024975-03), the Vanderbilt Ingram Cancer Center (P30 CA68485), the Vanderbilt Vision Center (P30 EY08126), and NIH/NCRR (G20 RR030956).

## Author contributions

R.C.H. and M.Z. conceived the studies. Y.P., S.C., Y.W., J.T., A.N., S.A.K., M.J., F.P., G.S., W.L., J.C.C. and S.W. performed the studies. A.F. provided human samples, R.C.H., M.Z., Y.P., C.B., M.W. and S.C. analyzed the results and produced the figures. Y.P., S.C., M.Z. and R.C.H. wrote the manuscript and R.C.H., M.Z., J.P.A.O., A.S.T. and A.F. edited the manuscript.

## Competing interests

The authors declare no competing interests.

## Additional information

**Supplementary information** The online version contains supplementary material available at <https://doi.org/10.1038/s41467-025-59393-y>.

**Correspondence** and requests for materials should be addressed to Ming-Zhi Zhang or Raymond C. Harris.

**Peer review information** *Nature Communications* thanks Haikuo Li, Andreas Linkermann and the other, anonymous, reviewer(s) for their contribution to the peer review of this work. A peer review file is available.

**Reprints and permissions information** is available at <http://www.nature.com/reprints>

**Publisher's note** Springer Nature remains neutral with regard to jurisdictional claims in published maps and institutional affiliations.

**Open Access** This article is licensed under a Creative Commons Attribution-NonCommercial-NoDerivatives 4.0 International License, which permits any non-commercial use, sharing, distribution and reproduction in any medium or format, as long as you give appropriate credit to the original author(s) and the source, provide a link to the Creative Commons licence, and indicate if you modified the licensed material. You do not have permission under this licence to share adapted material derived from this article or parts of it. The images or other third party material in this article are included in the article's Creative Commons licence, unless indicated otherwise in a credit line to the material. If material is not included in the article's Creative Commons licence and your intended use is not permitted by statutory regulation or exceeds the permitted use, you will need to obtain permission directly from the copyright holder. To view a copy of this licence, visit <http://creativecommons.org/licenses/by-nc-nd/4.0/>.

© The Author(s) 2025

## Acknowledgements

These studies were supported by NIH grants, DK51265, DK95785, DK62794, P30DK114809 (R.C.H., M.Z.), VA Merit Award 00507969